Journal of the Meteorological Society of Japan, Vol. 94, No. 2, pp. 151−183, 2016
DOI:10.2151/jmsj.2016-009

An Introduction to Himawari-8/9
— Japan's New-Generation Geostationary Meteorological Satellites

Kotaro BESSHO, Kenji DATE, Masahiro HAYASHI

Meteorological Satellite Center, Japan Meteorological Agency, Kiyose, Japan

Akio IKEDA

Satellite Program Division, Japan Meteorological Agency, Chiyoda, Japan

Takahito IMAI

Meteorological Satellite Center, Japan Meteorological Agency, Kiyose, Japan

Hidekazu INOUE, Yukihiro KUMAGAI, Takuya MIYAKAWA

Satellite Program Division, Japan Meteorological Agency, Chiyoda, Japan

Hidehiko MURATA

Meteorological Satellite Center, Japan Meteorological Agency, Kiyose, Japan

Tomoo OHNO

Satellite Program Division, Japan Meteorological Agency, Chiyoda, Japan

Arata OKUYAMA

Meteorological Satellite Center, Japan Meteorological Agency, Kiyose, Japan

Ryo OYAMA

Typhoon Research Department, Meteorological Research Institute, Tsukuba, Japan

Yukio SASAKI, Yoshio SHIMAZU

Satellite Program Division, Japan Meteorological Agency, Chiyoda, Japan

Kazuki SHIMOJI, Yasuhiko SUMIDA

Meteorological Satellite Center, Japan Meteorological Agency, Kiyose, Japan

Corresponding author: Kotaro Bessho, Data Processing Department, Meteorological Satellite Center, Japan Meteorological Agency, 3-235, Nakakiyoto, Kiyose, Tokyo 204-0012, Japan
E-mail: kbessho@met.kishou.go.jp

Masuo SUZUKI, Hidetaka TANIGUCHI,

Satellite Program Division, Japan Meteorological Agency, Chiyoda, Japan

Hiroaki TSUCHIYAMA

Volcanology Division, Japan Meteorological Agency, Chiyoda, Japan

Daisaku UESAWA

Meteorological Satellite Center, Japan Meteorological Agency, Kiyose, Japan

Hironobu YOKOTA, and Ryo YOSHIDA

Satellite Program Division, Japan Meteorological Agency, Chiyoda, Japan

(Manuscript received 3 April 2015, in final form 7 December 2015)

Abstract

Himawari-8/9–a new generation of Japanese geostationary meteorological satellites–carry state-of-the-art optical sensors with significantly higher radiometric, spectral, and spatial resolution than those previously available in the geostationary orbit. They have 16 observation bands, and their spatial resolution is 0.5 or 1 km for visible and near-infrared bands and 2 km for infrared bands. These advantages, when combined with shortened revisit times (around 10 min for Full Disk and 2.5 min for sectored regions), provide new levels of capacity for the identification and tracking of rapidly changing weather phenomena and for the derivation of quantitative products. For example, fundamental cloud product is retrieved from observation data of Himawari-8 operationally. Based on the fundamental cloud product, Clear Sky Radiance and Atmospheric Motion Vector are processed for numerical weather prediction, and volcanic ash product and Aeolian dust product are created for disaster watching and environmental monitoring. Imageries from the satellites are distributed and disseminated to users via multiple paths, including Internet cloud services and communication satellite services.

Keywords geostationary meteorological satellite; Himawari; satellite meteorology

1. Introduction

The Japan Meteorological Agency (JMA) launched its first Geostationary Meteorological Satellite (GMS) in 1977 (Kodaira et al. 1978) to join a satellite constellation under the Global Atmospheric Research Program (GARP), an international initiative established by the World Meteorological Organization (WMO) and the International Council of Scientific Unions (ICSU) in 1967. The constellation consisted of the GMS and satellites from the United States' National Aeronautics and Space Administration (NASA), its National Oceanic and Atmospheric Administration (NOAA), and the European Space Agency. Located at around 140°E, the GMS was equipped with an imager observing two bands (one for visible (0.50–0.75 μm) and one for infrared (10.5–12.5 μm)) and enabled continuous observation of atmospheric phenomena such as tropical cyclones, thunderstorms, heavy rainfall, and heavy snow in the East Asia and Western Pacific regions. A series of five GMS units were launched and operated until 2003. GMS-5 had an improved imager observing four bands (one for visible (0.72 μm) and three for infrared (6.75, 11.0, and 12.0 μm)), including a water vapor band. The GMS series were spin-stabilized units and are generally referred to as first-generation meteorological satellites. The satellite scheduled to follow GMS-5 was lost due to a launch vehicle failure, and the Geostationary Operational Environmental Satellite (GOES)-9 was used for backup operation from 2003 to 2005 in collaboration with NOAA/National Envi-

ronmental Satellite, Data, and Information Service (NESDIS).

Two Multi-functional Transport SATellites (MTSATs) succeeded the GMS series (JMA/MSC 2006; Miyamura 2007), fulfilling meteorological functions for JMA and aviation control functions for the Civil Aviation Bureau under Japan's Ministry of Land, Infrastructure, Transport and Tourism. The MTSAT imager had five observation bands (one for visible (0.675 μm) and four for infrared (3.75, 6.75, 10.8 and 12.0 μm)), and was more effective than the GMS-5 imager in detecting low-level cloud or fog at night. MTSAT-1R began operation in 2005, with MTSAT-2 having a period of operation from 2010 to 2015. The MTSAT series were created as three-axis body-stabilized satellites similar to the contemporary GOES series and are generally referred to as second-generation meteorological satellites. On the other hand, Meteosat Second Generation (MSG) operated by EUropean organisation for the exploitation of METeorological SATellites (EUMETSAT) is a spin-stabilized unit, but is also referred to as a second-generation meteorological satellite.

To enable uniform global earth observation, WMO promotes the World Weather Watch (WWW) program in collaboration with WMO member states. The space-based Global Observing System (GOS), which consists of geostationary meteorological satellites and low-earth-orbit meteorological satellites, plays an important role in the program. The GMS and MTSAT series have been indispensable parts of the GOS, providing cloud and water vapor imagery to more than 30 countries and territories, contributing to weather forecasts and natural-disaster countermeasures, and supporting safer transportation in the East Asia and Western Pacific regions. The GMS and MTSAT series are also called the Himawari series (himawari means "sunflower" in Japanese).

Himawari-8 was successfully launched from Japan's Tanegashima Space Center using an H-IIA rocket on 7 October 2014 and settled in geostationary orbit on 16 October. JMA has commenced the unit's operation from 7 July 2015. Himawari-9 will also be launched in 2016 for in-orbit standby service and will eventually replace Himawari-8. The Himawari-8/9 units are shown in Fig. 1. Both satellites will be operational for seven years, with Himawari-9's observation work continuing to 2029 (Fig. 2). JMA's Himawari-8/9 will enter service ahead of other third-generation meteorological satellites such as NOAA/NASA's GOES-R unit and EUMETSAT's Meteosat Third Generation (MTG) unit (Mohr 2014).

Fig. 1. Himawari-8/9.

This paper provides an overview of the Himawari-8/9 satellites. First, the basic functions and specifications are outlined in Section 2. Section 3 describes the ground segment for the new satellites. A detailed account of the new Himawari-8/9 imager is given in Section 4. In Section 5, JMA's Himawari-8/9 imagery and data distribution/dissemination scheme is explained. Section 6 shows physical retrieval products created from satellite observation data. In Section 7, the development plan for new products and application of Himawari-8/9 observation data are discussed. Section 8 summarizes the paper.

2. Functions and specifications

Himawari-8/9 have identical specifications as listed in Table 1. They are three-axis attitude-controlled satellites with a length of approximately 8 meters and a mass of approximately 3,500 kg each at launch. Their buses were made by Mitsubishi Electric, and both will be located at 140.7°E. The satellites' highly improved Advanced Himawari Imagers (AHIs) have capabilities comparable to those of the Advanced Baseline Imager (ABI) on board GOES-R, which is run under a collaborative program between NOAA and NASA (Schmit et al. 2005; Schmit et al. 2008). A description of the AHIs (made by Harris/Exelis) is given in Section 4. Himawari-8/9 use the Ku-band for telemetry and command operations and

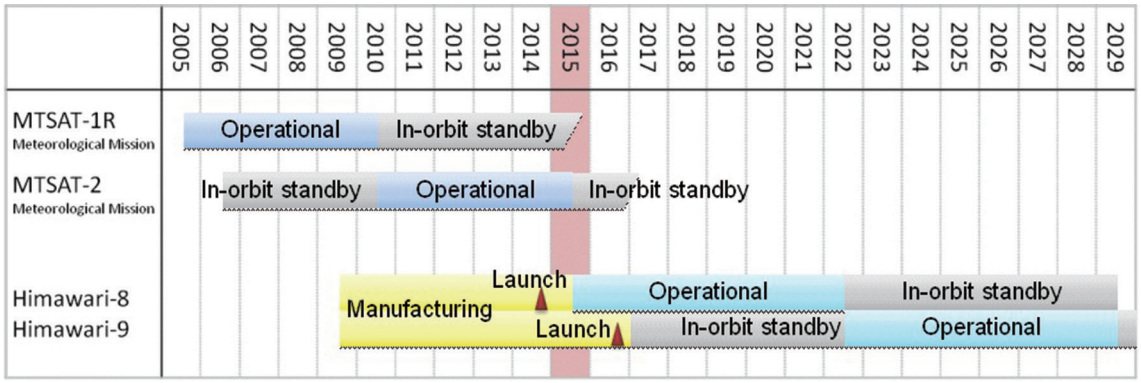

Fig. 2. Himawari-8/9 schedule.

Table 1. Major specifications of Himawari-8/9.

Attitude control	3-axis stabilization
Size during operation	Total length: approx. 8 m
Mass	Dry mass: approx. 1300 kg
	At launch: approx. 3500 kg
Design lifetime	Meteorological mission: 8 years or longer
	Satellite: 15 years or longer
Geostationary position	140.7 degrees east
Imager	Advanced Himawari Imager (AHI)
Space environment monitor	Space Environment Data Acquisition Monitor (SEDA).
Communications	1) AHI data transmission Ka-band, 18.1 – 18.4 GHz (downlink)
	2) Data Collection System (DCS) Uplink from Data Collection Platforms (DCPs) 402.0 – 402.4 MHz (uplink) Transmission to ground segments Ka-band, 18.1 – 18.4 GHz (downlink)
	3) Telemetry and command Ku-band, 13.75–14.5 GHz (uplink) 12.2–12.75 GHz (downlink)
Contractor	Mitsubishi Electric Corporation
Launch vehicle	H-IIA rocket

the Ka-band for downlinking of AHI data. Each satellite also carries a transponder to relay meteorological and tide/tsunami data from earth-based observing stations (Data Collection Platforms, or DCPs) in order to sustain the Data Collection System (DCS) of the GMS and MTSAT series. JMA's geostationary meteorological satellites have taken on a much more significant carrier role since the Great Sumatra-Andaman Earthquake of 2004, the Great East Japan Earthquake of 2011, and numerous torrential rain-related disasters in Japan.

Himawari-8/9 have a Space Environment Data Acquisition monitor (SEDA) to observe high-energy electrons and protons in orbit. JMA will internally use

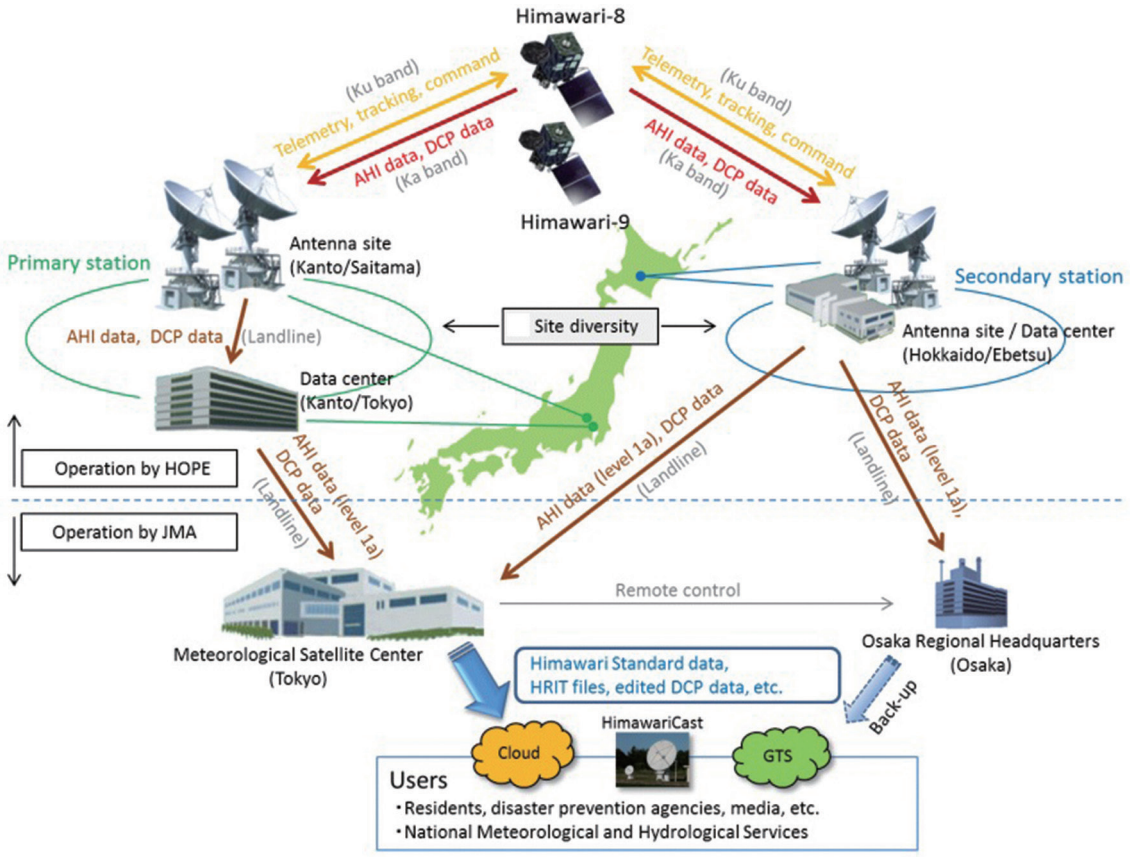

Fig. 3. Overview of ground segment for Himawari-8/9.

the data obtained in this way to support satellite operation and failure analysis. The SEDA unit, supplied by RUAG Space, is based on the EMU (Environmental Monitoring Unit) developed for the Galileo satellites. The data it collects are provided by JMA on a near-real-time basis to the National Institute of Information and Communications Technology (NICT), which leads space weather research in Japan.

3. Ground segment

Himawari-8/9 and related ground equipment are operated by Himawari OPeration Enterprise corporation (HOPE)—a special-purpose company established under a Private Finance Initiative (PFI) project. HOPE controls the satellites as well as receiving data derived from their AHI/DCP units and sending the data to JMA, which processes the information and provides related products to users. Figure 3 highlights the Himawari-8/9 ground segment.

As mentioned previously, the Ku-band is used for telemetry, tracking, and command of Himawari-8/9, and the Ka-band is used for data downlinks from their AHI and DCP units. To minimize the adverse effects of rain attenuation on these bands, antenna sites approximately 800 km apart are situated in the Kanto (primary station) and Hokkaido (secondary station) regions of Japan for diversity. Data centers are located in the vicinity of these sites to process the received data.

Each antenna site has transmitting/receiving equipment consisting of two antennas with diameters of 9 meters, and the data centers have equipment for satellite control and for processing of AHI/DCP data received at the antenna sites. AHI data are processed to level 1a data (known as Himawari radiometric data, which are raw data with calibration and navigation parameters attached), while DCP data are formatted for JMA's telecommunications system. The data processed at these centers are sent to JMA's Meteorological Satellite Center (MSC) and JMA's Osaka Regional Headquarters (referred here simply as "Osaka"). If the primary data center in Kanto should

Table 2. Himawari-8/AHI and MTSAT-2/Imager specifications.

	Himawari-8/AHI			MTSAT-2/Imager		
	Band #	Wavelength (μm)	Spatial resolution (km)	Band	Wavelength (μm)	Spatial resolution (km)
Visible	#1	0.47	1			
	#2	0.51				
	#3	0.64	0.5	VIS	0.68	1
Near-infrared	#4	0.86	1			
	#5	1.6	2			
	#6	2.3				
Infrared	#7	3.9		IR4	3.7	4
	#8	6.2		IR3	6.8	4
	#9	6.9				
	#10	7.3				
	#11	8.6				
	#12	9.6				
	#13	10.4		IR1	10.8	4
	#14	11.2				
	#15	12.4		IR2	12.0	4
	#16	13.3				

become dysfunctional, the secondary one in Hokkaido will take over its duties.

MSC and Osaka have computer systems exclusively for processing data from the centers. Himawari radiometric data received at MSC from both centers are interpolated, compared, and selected. Level 1b Himawari Standard Data (HSD), High-rate Information Transmission (HRIT) files, and edited DCP data are then produced and provided to users. Osaka receives data only from the secondary data center and will issue satellite data and products if the MSC system should become dysfunctional due to regional infrastructure issues caused by natural disasters or similar.

4. AHI instruments

The AHIs on board Himawari-8/9 are greatly improved over those of the MTSAT series in terms of the number of bands, spatial resolution and temporal frequency. AHIs have 16 observation bands (three for visible, three for near-infrared, and ten for infrared), whereas the MTSAT series imagers have five bands. Table 2 shows details of the Himawari-8/AHI and MTSAT-2/Imager bands along with the related wavelengths, and Fig. 4 shows their spectral response functions (SRFs) compared with those for MTSAT-2 bands. The performance of the AHI on board Himawari-8 is evaluated in ground testing. The test results, including data on the center wavelength, bandwidth, bits, Signal-Noise Ratio (SNR), dynamic range, radiometric calibration accuracy, Internal Calibration Target (ICT) emissivity, and out-of-band response, can be found on the website at http://www.data.jma.go.jp/mscweb/en/himawari89/space_segment/doc/AHI8_performance_test_en.pdf.

4.1 Individual band characteristics

Each AHI band has its own characteristics. True-color images from a combination of the three visible bands (blue: #1, 0.47 μm; green: #2, 0.51 μm; red: #3, 0.64 μm) appear as if seen by the human eye. Figure 5 shows the first true-color composite image from Himawari-8 at 02:40 UTC on 18 December 2014. The first images in all bands of Himawari-8 can be found

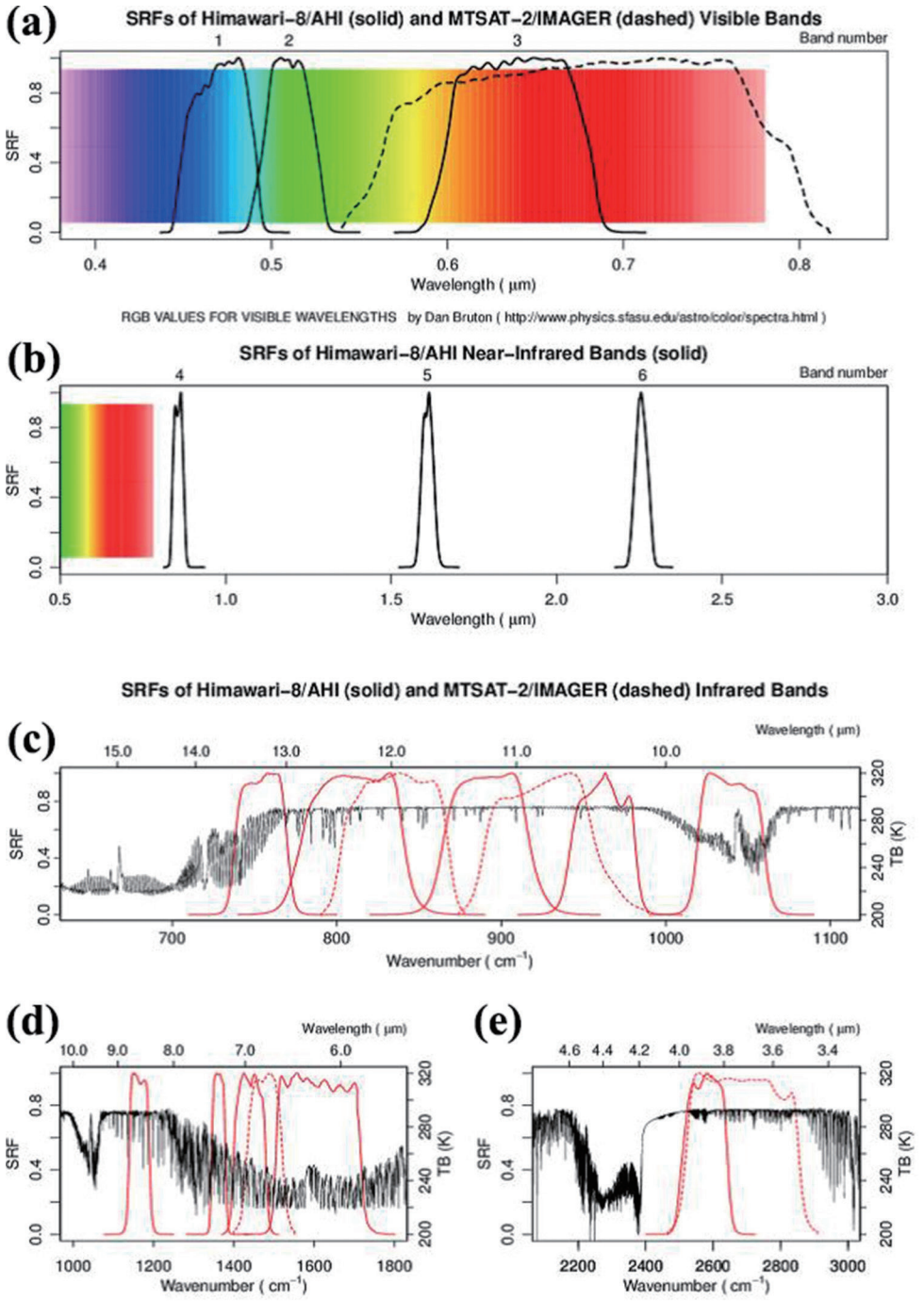

Fig. 4. SRFs for visible bands (a), near-infrared bands (b), and infrared bands (c-e) of the AHI unit on board Himawari-8 and the Imager unit on board MTSAT-2. The solid and dashed black lines in the visible/near-infrared band panels (a and b) represent values for AHI and Imager, respectively, and the corresponding red lines represent the same in the infrared band panels. The RGB spectra in the visible/near-infrared band panels (a and b) were generated using the program provided at http://www.physics.sfasu.edu/astro/color/spectra.html. The black lines in the infrared panels (c-e) represent the brightness temperatures of up-welling radiances at the top of the atmosphere as simulated using the radiative transfer model (LBLRTM) with HITRAN2000 (AER updates) line parameters based on the US standard atmosphere.

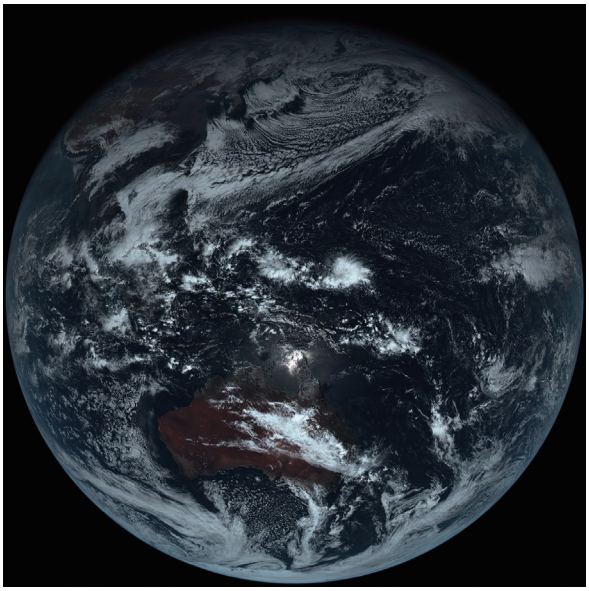

Fig. 5. First true-color composite image from Himawari-8 at 02:40 UTC on 18 December 2014.

on the website at http://www.jma.go.jp/jma/jma-eng/satellite/news/himawari89/20141218_himawari8_first_images.html. Near-infrared (NIR) bands #4–6 (0.86, 1.6, and 2.3 μm) provide cloud physical parameter data such as information on the water/ice phase, particle size, and optical thickness. Solar reflectance differences in the visible and NIR bands enable the collection of surface property data such as information on snow/ice cover and vegetation. The shortwave infrared band #7 (3.9 μm), which is inherited from the MTSAT series, is used to monitor low-level cloud, fog, wildfires, and other phenomena. Three bands from #8–10 (6.2, 6.9, and 7.3 μm) in the water vapor absorption band are available, as opposed to the single band of the MTSAT series. The water vapor bands are sensitive to middle-to-upper tropospheric humidity, and differences in sensitivity between them provide humidity vertical profile information. Band #11 (8.6 μm) is used for thin ice cloud monitoring in conjunction with other atmospheric window bands. Bands #10 and #11 are sensitive to volcanic SO_2 gas. Band #12 (9.6 μm), which is in the ozone absorption band, is used to monitor stratospheric ozone and (indirectly) potential vorticity. There are three bands (#13–15; 10.4, 11.2, and 12.4 μm) in the 10–12 μm atmospheric window as opposed to the two (known as "split window bands") of the MTSAT series. These are used to monitor ice crystals/water, lower water vapor, volcanic ash, sea surface temperature, and other phenomena. The atmospheric window band is present on most meteorological satellites and is mainly used at operational weather centers to support real-time weather analysis and forecasting. Band #16 (13.3 μm), which is in the CO_2 absorption band, is used for cloud top height assignment and the estimation of thin cirrus opacity.

4.2 Spatial resolutions

Table 2 also lists the AHI sub-satellite spatial resolutions. The highest resolution is 0.5 km at sub-satellite point for band #3 in the visible wavelength. Those of other visible bands and band #4 in the near-infrared wavelength are 1 km. Other near-infrared bands and all infrared bands have spatial resolutions of 2 km. The values for AHI visible and infrared bands are twice of those of MTSAT-2/Imager. Figure 6 shows the spatial resolution difference between the visible band of MTSAT-2/Imager and band #3 of Himawari-8/AHI at 03:00 UTC on 29 January 2015. From the imagery of Himawari-8/AHI, each cumulus cloud is distinguished clearly.

4.3 Observation areas and frequencies

Figure 7 shows 10-min timelines of AHI observation areas and frequencies. The five scans performed by the AHIs are Full Disk, Japan Area (Regions 1 and 2), Target Area (Region 3), and two Landmark Areas (Regions 4 and 5). The scan ranges for Full Disk and the Japan Area are preliminarily fixed, while those for the Target Area and Landmark Areas are flexible to enable prompt response to meteorological conditions. Initial Himawari-8 operation involves the use of both sets of Landmark Area data exclusively for navigation and moon observations for calibration; the data are not intended for use in satellite products. In future work, JMA plans to use one Landmark Area (Region 5) for observation of phenomena such as rapidly developing cumulonimbus cloud and to provide the resulting data to users for watching the localized torrential rain brought by the cloud. On a specific timeline, the AHIs scan the Full Disk once, the Japan Area and Target Area four times, and each Landmark Area twenty times. Accordingly, Full Disk images are taken every 10 min, Japan Area and Target Area images every 2.5 min, and Landmark Area images every 30 s. In Himawari-8/9 baseline observation, the timeline is repeated every 10 min other than in housekeeping operation. Supplement 1 shows infrared (IR1 or band #13) animations from MTSAT-2 Northern Hemisphere images every 30 min (left)

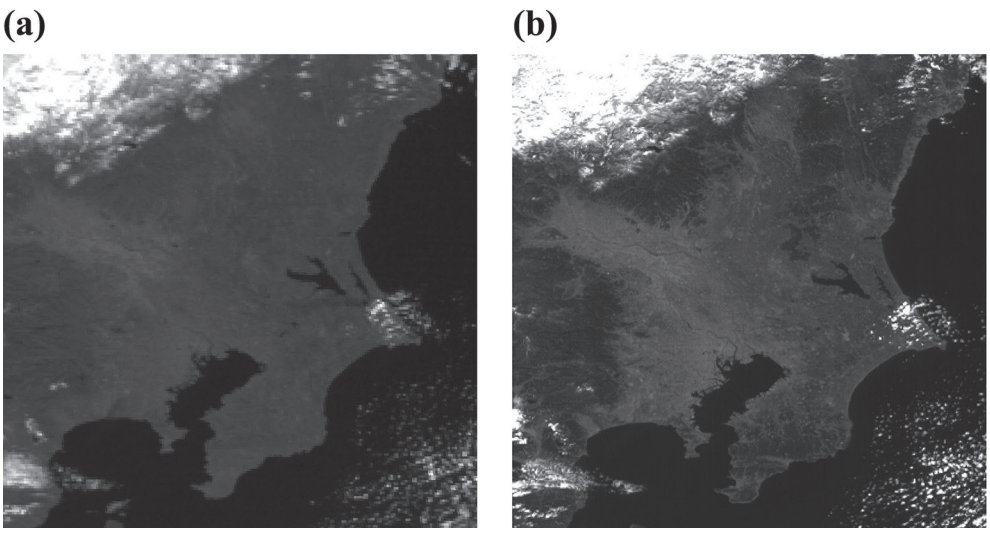

Fig. 6. Sample of spatial resolution difference between the visible band of MTSAT-2/Imager (a) and band #3 of Himawari-8/AHI (b) on 03:00 UTC on 29 January 2015.

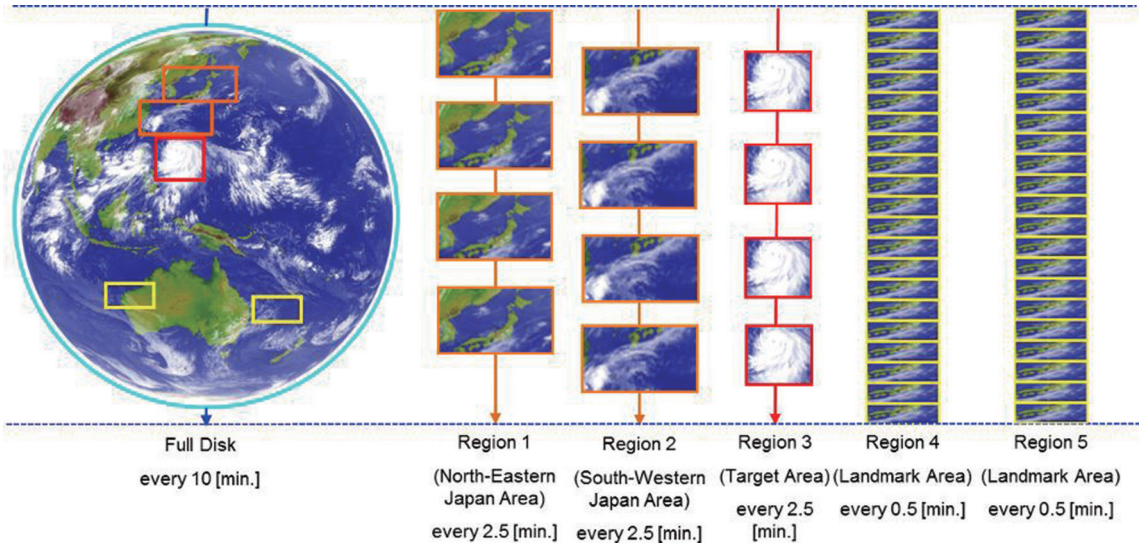

Fig. 7. AHI observation areas and frequencies on a timeline of 10 min.

and Himawari-8 Japan Area images every 2.5 min at 11:00–19:30 UTC on 26 January 2015. Synoptic scale cloud motions can be detected from the images taken at 30-min intervals. On the other hand, mesoscale cloud motions can be followed on the images taken every 2.5 min. From these animations, the advantage of high temporal frequency of Himawari-8/AHI is confirmed.

4.4 Sample observation data and simulated data

To support the development of Himawari-8/9 products, sample observation data created from AHI observation data and simulated proxy satellite observations derived from numerical modeling have been provided on the website at http://www.data.jma.go.jp/mscweb/en/himawari89/space_segment/spsg_sample.html. The AHI observation data set is acquired in Himawari-8 in-orbit-test period, not during its opera-

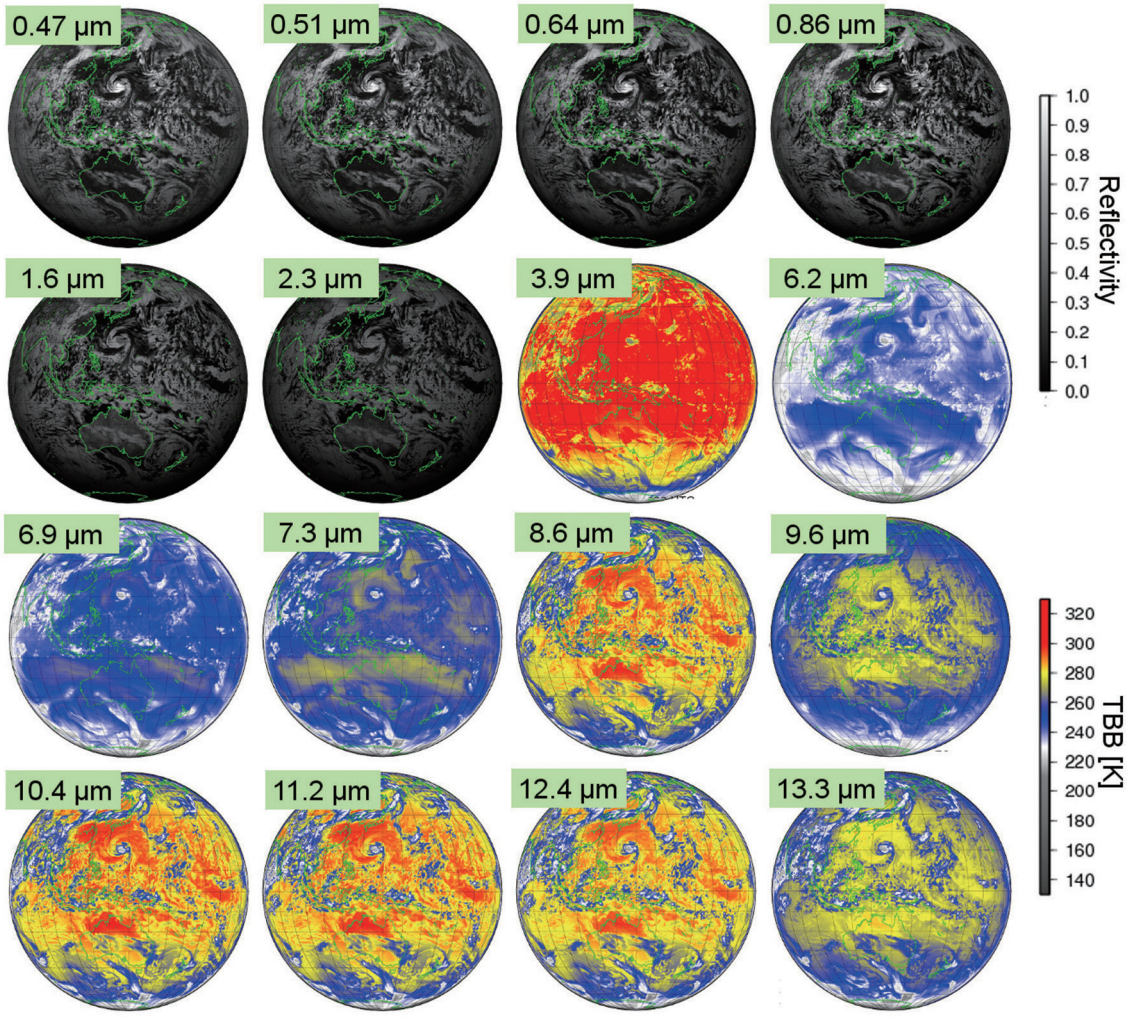

Fig. 8. Simulated images for Himawari-8's 16 AHI bands based on RSTAR.

tion. In the website, there are some source codes for reading and converting the sample data.

Figure 8 shows an example of AHI 16-band simulated observation using a radiative transfer model based on the provisional response functions of the imaging units. Table 3 shows radiative transfer calculation design based on the System for Transfer of Atmospheric Radiation (RSTAR) package (Nakajima and Tanaka 1986; Nakajima and Tanaka 1988; Stamnes et al. 1988). Analysis and forecasts from JMA's Numerical Weather Prediction (NWP) Global Spectral Model (GSM) (Japan Meteorological Agency 2013) were adopted as atmospheric fields. Since February 2013, these proxy data have been available on the MSC website at http://www.data.jma.go.jp/mscweb/en/himawari89/space_segment/spsg_ahi_proxy.html.

For users planning to utilize only bands similar to those of MTSAT-2 after Himawari-8 becomes operational, Himawari-8/AHI bands compatible with those of MTSAT-2/Imager are selected. Bands #3, 7, 8, 13, and 15 of the AHIs are considered compatible with the VIS, IR4, IR3, IR1, and IR2 specifications of MTSAT-2/Imager, as shown in Table 2. In this selection of compatible bands, the simulated satellite observations mentioned above were used to compare Himawari-8/AHI with MTSAT-2/Imager (Murata et al. 2015).

Table 3. Radiative transfer calculation design.

Radiative Transfer Model (RTM)	Rstar6b (Nakajima and Tanaka 1986)
Longitude of sub-satellite point	140.0 degrees east
Spectral Response Function (SRF)	Approximated with five points
Number of vertical layers in RTM	14
Atmospheric profile	GSM (TL959L60, 20-km horizontal resolution) (JMA 2013)
Surface wind speed	GSM
Surface reflectance	MODIS product (MOD09)
Aerosol	Total-column climatology value used in the GSM
Cloud	Retrieved from GSM cloud liquid/ice water content (Ice crystal habits: hexagonal plates, Yang et al. 2000)
Ozone	3D climatological ozone used in the GSM (Maki et al. 2008)

4.5 Image navigation and registration

To support accurate image navigation and registration (INR), the Himawari-8/9 satellites have star trackers (STTs), inertia reference units (IRUs), and angular rate sensors (ARSs) installed on optical benches together with their AHIs for attitude determination. These sensors help to suppress the influence of thermal strain by the optical benches, and integrally mounted sensors on the bench reduce alignment errors between them. To mitigate the thermal strain, a carbon fiber–reinforced plastic panel with low thermal expansion is used for the optical bench. In addition, the IRUs and ARSs are equipped close to the AHI to ensure its directional accuracy.

The INR process in the Himawari-8/9 ground processing system mainly involves the use of orbit and attitude information. The orbit parameters are determined by ranging, and related prediction is used for image navigation. To determine attitude, the STT sensors identify and track stars in the field of view. The IRUs and ARSs are angular velocity sensors. The IRUs measure drifts of attitude with variations lower than 10 Hz, and the ARSs detect jitters higher than 10 Hz. The STTs' sampling rate is 4 Hz, the IRUs' is 128 Hz, and the ARSs' is 512 Hz.

To determine errors in the orbit and attitude established, landmark analysis (i.e., pattern matching between the database coastline and that of observation images) is also used. These errors are compensated as attitude bias and image distortion. Band-to-band co-registrations are determined via direct pattern matching between different bands, and real-time correction is performed in reference to the relationship between these co-registrations and AHI optical system temperatures. The typical residual error after the co-registration process varies diurnally. The variation is about 2.5 pixels for band #5 and about 0.5 pixels for other VIS and NIR bands. For IR bands, the variation is 0.1 pixels at the largest.

4.6 Calibration

For detector sample calibration, the AHIs have a blackbody as the ICT and a solar diffuser as a Solar Calibration Target (SCT). The ICT is temperature-controlled using heaters and generates a constant radiance. The SCT is the first solar diffuser installed on any JMA geostationary meteorological satellite imager and is made of Spectralon (manufactured by Labsphere). The MODerate resolution Imaging Spectroradiometer (MODIS) of the Aqua/Terra satellites has the same equipment for its on-board calibrator to reflect and diffuse sunlight for observation by detectors. The required accuracy of solar calibration is within 5 % radiance. According to Xiong et al. (2004), the expected accuracy is within 2 % reflectance and 5 % radiance. The ICT is used as a hot reference along with space view observations as a cold reference for the IR bands. Meanwhile, the SCT is used as a

bright reference for the VIS and NIR bands together with space view observations as dark references. Using these calibration targets, linear and bias calibration coefficients are derived to convert counts of raw detector sample data into radiances. After solar diffuser stability checking was completed on June 2015, calibration coefficients were updated based on the observation results from SCT in the visible/near-infrared bands. In this stability checking, JMA plans to perform lunar observation for long-period stable references (Kieffer and Stone 2005).

To check the quality of the data obtained, JMA has developed visible and infrared vicarious calibration methods under the framework of the Global Space-based Inter-Calibration System (GSICS) (Goldberg et al. 2011) and collaborative research with the University of Tokyo's Atmosphere and Ocean Research Institute (AORI). The infrared calibration approach developed under the GSICS project utilizes hyper-spectral infrared sounders (hyper sounders) such as the Infrared Atmospheric Sounding Interferometer (IASI) on board EUMETSAT's Metop satellite and the Atmospheric InfraRed Sounder (AIRS) on board NASA's Aqua satellite (Gunshor 2006; Tobin 2006; Tahara 2009). The approach for comparison of imagers on board geostationary satellites with hyper sounders involves generating a super channel which clones the broad channel of the hyper sounder by minimizing the spectral response difference. This method supports the investigation of sensor bias and its seasonal or diurnal variation. The MSC website (http://www.data.jma.go.jp/mscweb/data/monitoring/calibration.html) highlights calibration monitoring for Himawari-8 and the MTSAT series based on this approach. Visible/near-infrared band calibration methods are also being examined within the GSICS framework. JMA has further developed an approach for visible/near-infrared vicarious calibration as part of collaborative research with AORI. The technique is based on radiative transfer computation above spatially uniform targets such as cloud-free ocean areas and liquid cloud top (Kosaka 2012). Information on the imager sensitivity trend of Himawari-8 and MTSAT-2 is also provided on the same MSC website. JMA plans to validate AHI sensor characteristics based on these approaches. AHI fundamental performance in-orbit-test (e.g., radiometric calibration accuracy and SNR) is summarized in Okuyama et al. (2015).

The AHIs have temperature sensors on their mirrors and other inner structures. The use of data from these sensors in ground segment processing enables JMA to apply the Midnight Blackbody Calibration Correction (MBCC) algorithm (Weinreb and Han 2003) to offset nighttime effects of blackbody in the same way as the GOES imagers (Johnson and Weinreb 1996). However, no significant nighttime effect in the AHIs and their blackbodies is expected.

5. Level-1B products and data distribution/dissemination

JMA processes satellite-derived level-1a Himawari radiometric data to create HSD as a level-1b product in Himawari Standard Format (HSF). HSD are used as master data for all Himawari-8/9 products. Details of HSD and HSF are provided on the MSC website at http://www.data.jma.go.jp/mscweb/en/himawari89/space_segment/spsg_sample.html. Himawari-8/9 imagery in other data formats such as HRIT, Low Rate Information Transmission (LRIT), Portable Network Graphics (PNG), and Network Common Data Form (NetCDF) is also processed from HSD and provided by JMA via multiple paths. Sample data created in various formats from AHI observation and proxy data can be found on the same website.

Imagery from MTSAT-2 satellite is provided via MTSAT-1R direct dissemination through the L-band frequency HRIT and LRIT services. Most National Meteorological and Hydrological Services (NMHSs) in the East Asia and Western Pacific regions receive this imagery using L-band antennas and receivers and process it with dedicated systems. JMA also provides the same HRIT service imagery via the online JMA Data Dissemination System (JDDS).

Himawari-8/9 do not carry equipment for direct dissemination, as detailed in Section 2. Instead, all imageries derived from the satellites are distributed to NMHSs via the HimawariCloud service. JMA also runs the HimawariCast service, by which primary sets of imagery are disseminated to users via a communication satellite using Digital Video Broadcasting-Satellite-Second Generation (DVB-S2) technology. This section covers the distribution/dissemination paths used by JMA.

5.1 HimawariCloud service

To distribute the enormous volumes of imagery that Himawari-8/9 produce, in April 2015, JMA established an Internet cloud service (HimawariCloud) for NMHSs in the East Asia and Western Pacific regions. Table 4 shows the data set distributed via this service. HSD are provided as core data with 16 bands and the finest spatial resolution. The true-color images detailed in Section 4 are provided in PNG format.

Table 4. Data set distributed via the HimawariCloud service.

Format	Observation area	Notes
Himawari Standard Data	Full Disk Target Area	- Interval: 10 min (Full Disk); 2.5 min (Target Area) - Number of bands: 16 - Spatial resolution: VIS: 0.5–1 km; NIR: 1–2 km: IR: 2 km
Portable Network Graphics (PNG)	Full Disk Target Area	- True-color images (composites of three visible bands) - Interval: 10 minutes (Full Disk); 2.5 min (Target Area) - Spatial resolution: 1 km
Network Common Data Form (NetCDF)	Target Area	- Interval: 2.5 min - Number of bands: 16 - Spatial resolution: VIS: 0.5–1 km, NIR: 1–2 km; IR: 2 km

Table 5. Data set continuously distributed via JDDS.

Format	Observation area	Notes
HRIT files	Full Disk	- Format compatible with the MTSAT series HRIT service - Interval: 30 minutes - Number of bands: 5 (VIS: 1; IR: 4) - Spatial resolution: VIS: 1 km; IR: 4 km

For rapid scanning observation, imagery in NetCDF is also created and distributed. NMHSs are able to access the cloud and retrieve data using an HTTP 1.1 client such as a Web browser or a Wget command. It should be noted that an Internet connection with a speed of at least 20 Mbps is required to download all HSD. These data are separately created for each band and divided into 10 segments from north to south so that NMHSs can select only the files necessary for their operations.

Several Japanese universities and research organizations have received Himawari-8/9 data via the HimawariCloud service and re-distributed them for research purposes. These are not JMA organizations; their services are based on voluntary work and are conducted on a best-effort basis.

To support service continuity for JDDS users, JMA also produces HRIT files compatible with MTSAT data (Table 5). These feature five bands near the MTSAT observation bands and are provided every 30 min with the same frequency as the MTSAT service.

5.2 HimawariCast service

The HimawariCloud service requires high-speed Internet access, whereas the HimawariCast service is suitable for users with limited Internet connections. Table 6 shows the data set disseminated via communication satellite. HRIT files represent the core data of the service, and LRIT files are also included to support LRIT service users. The dissemination further includes meteorological data other than Himawari imagery in SATellite Animation and Interactive Diagnosis (SATAID) format. JMA's SATAID visualization software enables the display and analysis of satellite images with other meteorological data. A sample SATAID viewer image is shown in Fig. 9. SATAID enables the superimposition of various data and products, such as NWP information and in-situ observation data, onto satellite imagery. It is widely used by NMHSs in the East Asia and Western Pacific regions as an operational tool for daily weather analysis and forecasting due to its usefulness and convenience.

The HimawariCast receiving and processing system includes a C-band antenna system, a Low Noise Block converter (LNB), a DVB-S2 receiver, and a

Table 6. Data set distributed via the HimawariCast service.

Data type	Format	Notes
Himawari imagery (Full Disk)	HRIT files	- Format compatible with the MTSAT series HRIT services - Interval: 10 min - Number of bands: 14 (VIS: 1; NIR: 3; IR: 10) - Spatial resolution: VIS: 1 km; NIR: 4 km; IR: 4 km
	LRIT files	- Format compatible with the MTSAT series LRIT services - Interval: 10 min - Number of bands: 4 (VIS: 1; IR: 3) - Spatial resolution: 5 km
NWP products (GPV)	SATAID format	- JMA Global Spectral Model (GSM) products - Interval: 6 hr
In-situ observations (surface stations, ships, radiosondes)	SATAID format	- Observational data for the East Asia and Western Pacific regions
ASCAT ocean surface wind	SATAID format	- Observational data from EUMETSAT's Metop polar-orbiting satellites

desktop computer with data casting client software and visualization software. More information on the system can be found at http://www.data.jma.go.jp/mscweb/en/himawari89/himawari_cast/himawari_cast.html.

JMA's HimawariCast service started in January 2015 with MTSAT-2 still in operation. MTSAT-2 imagery was disseminated through the service in parallel with direct dissemination via MTSAT-1R until the start of Himawari-8 operation. From July 2015, Himawari-8 data imagery has been disseminated operationally via the HimawariCast service.

5.3 WMO Information System Portal

JMA operates the WIS Portal website as the Tokyo Global Information System Centre (GISC-Tokyo) of the WMO Information System (WIS). Himawari-8 imagery in SATAID format and the meteorological data shown in Table 7 are provided through the SATAID service, which is a data distribution initiative of GISC-Tokyo. The Internet-based SATAID service and HimawariCast data delivered via a communication satellite are provided on a complementary basis for SATAID users.

5.4 JMA website

JMA provides Himawari-8 imagery in PNG format on its website for public consumption. To facilitate rapid downloading of essential imagery for meteorological services, the Agency also formulates various types of cut-out imagery in Joint Photographic Experts Group (JPEG) format on its website:

http://www.jma.go.jp/en/gms/
http://www.jma.go.jp/en/gms150jp/
http://www.data.jma.go.jp/mscweb/data/himawari/index.html

6. Level-2 products and contribution to climate research activity

The imagers on board the MTSAT second-generation geostationary meteorological satellites have five observation bands (one for visible and four for infrared). Using imagery from these bands, JMA monitors synoptic-scale meteorological phenomena such as extratropical cyclones, Baiu front activity, and tropical cyclones to help mitigate the effects of meteorological disasters. The best practice of these efforts involves employment of the Dvorak method to enable estimation of tropical cyclone intensity (Dvorak 1975, 1984; Velden et al. 2006). The Objective Dvorak Method was also developed by Velden et al. (1998) and Olander and Velden (2007). The Dvorak method is used by the Regional Specialized Meteorological Centre (RSMC) Tokyo to analyze the intensity of typhoons based on satellite observation. In 2013, RSMC Tokyo has also started the practical

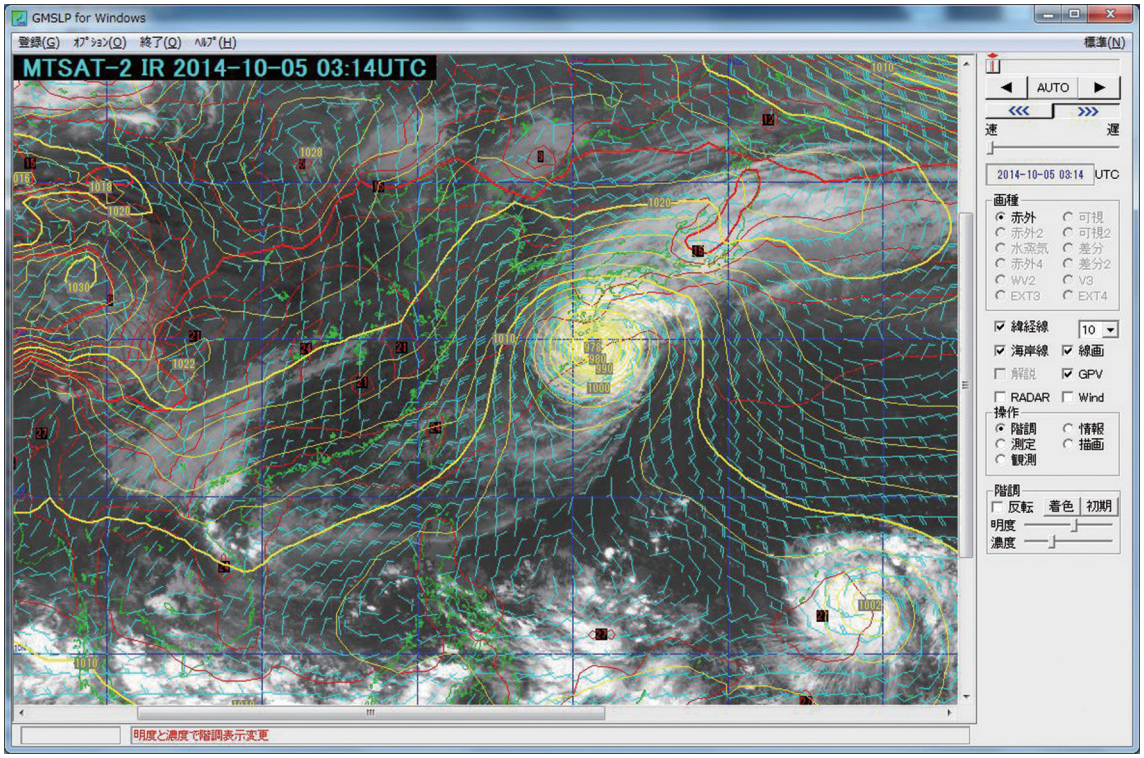

Fig. 9. SATAID viewer image. Satellite infrared imagery (black and white) is visualized with contours of surface pressure (yellow), surface air temperature (red), and wind barbs (blue) from NWP.

Table 7. Data set distributed via GISC-Tokyo's SATAID service .

Data type	Format	Notes
Himawari imagery (cut-out from Full Disk)	SATAID format	- Interval: 10 min - Number of bands: 5 (VIS: 1; IR: 4) - Spatial resolution: 4 km
NWP products (GPV)	SATAID format	- JMA Global Spectral Model (GSM) products - Interval: 6 hr
In-situ observations (surface stations, ships, radiosondes)	SATAID format	- Observational data for the East Asia and Western Pacific regions
ASCAT ocean surface wind	SATAID format	- Observational data from EUMETSAT's Metop polar-orbiting satellites

use of the Objective Dvorak Method (Kishimoto et al. 2013). From the start of the operation of Himawari-8, the method has been applied to its data set. To obtain maximal use from the data of new-generation geostationary satellites such as Himawari-8/9 and GOES-R, the Objective Dvorak Method is being updated (Goodman et al. 2012).

Level-2 physical products are also utilized in JMA's work, as exemplified by the indispensable role played by Clear Sky Radiance (CSR) and Atmospheric Motion Vector (AMV) data from MTSAT in the initialization of NWP. For aviation operators, JMA/MSC provides volcanic ash information from the satellites to the Tokyo Volcanic Ash Advisory Center

(VAAC). MTSAT environmental products such as data on dust presence, sea surface temperature estimation, and retrieval of sea ice motion vectors also play a significant role in JMA's operations.

As described in Section 4, Himawari-8/9 offer high observation potential to support users in the development and improvement of various physical products. Previous satellite products such as cloud property, CSR, and AMV information have been improved using AHI data. JMA also uses these data in the development of new retrieval algorithms for products relating to cloud-free areas, such as data on aerosol properties with a focus on volcanic ash and dust. The sections below briefly outline basic meteorological products developed by JMA from Himawari-8/9 AHI data in collaboration with geostationary meteorological satellite employment organizations such as NOAA/NESDIS and EUMETSAT. JMA and these organizations are members of the Coordination Group for Meteorological Satellites (CGMS), which consists of developers and operators of meteorological satellites, space agencies operating research and developing satellites, and WMO.

In addition to the geophysical products listed above, JMA contributes to international climate research frameworks such as the International Satellite Cloud Climatology Project (ISCCP), the Global Precipitation Climatology Project (GPCP), and the Sustained, Co-Ordinated Processing of Environmental satellite data for Climate Monitoring (SCOPE-CM) initiatively by providing geostationary meteorological satellite observation data and products. These activities are also briefly outlined below.

6.1 Fundamental cloud product

Cloud property information is a highly essential meteorological product derived from satellite observations, not only because it is used for weather analysis, but also because it is applied in the retrieval of other products (e.g., CSR and AMV). For example, masking the cloud area is the first step in the determination of surface parameters in satellite remote sensing. Considering the importance of cloud property information, JMA is currently operating and developing two cloud products with data from Himawari-8/9. One is based on a statistical approach, and the other involves a physical (1D-Var) approach. This section outlines the cloud product using the former, and the latter is described in Section 7.1.

The fundamental cloud product based on the statistical approach provides data on cloud mask, cloud top height, cloud type, and phase for each pixel of the Himawari-8/9 infrared bands (2 km at the sub-satellite point). The algorithm is based on methods developed by the Nowcasting Satellite Application Facility (Meteo-France 2012). It involves the use of a threshold technique with brightness temperature and reflectivity for cloud mask and cloud type/phase retrieval. It also incorporates "a local radiative center" and a threshold tuning method developed by NOAA/NESDIS (Heidinger 2011). The interpolation, intercept (Szejwach 1982), and radiance rationing methods (Menzel et al. 1983) are applied for cloud height assignment. The fundamental cloud product algorithm involves the use of radiative transfer calculation results obtained from NWP data to determine thresholds for CSR from infrared bands. A prototype product was made using MSG/Spinning Enhanced Visible and InfraRed Imager (SEVIRI) data (Schmetz at al. 2002). Table 8 shows evaluation results for the prototype cloud mask, cloud top height, cloud type, and phase compared with the Aqua/MODIS Level2 products (MYD35_L2 and MYD06_L2) as references. Evaluation was performed over periods of two weeks in each season (28 December 2011–10 January 2012, 28 March 2012–10 April 2012, 27 June 2012–10 July 2012, and 27 September 2012–10 October 2012), and scores were calculated using temporally and spatially matched MODIS products within the four periods. Accuracy and hit rate are defined as (A+D)/(A+B+C+D) and A/(A+B), respectively, and shown in Table 8 (d). Cloud mask detection accuracy was 85 %, and most of the other scores were also reasonable. However, the evaluation results also suggest the need for further improvement in cloud detection over snow/ice areas and cloud height assignment for semi-transparent cloud.

6.2 CSR product

The CSR product provides area-averaged radiances and brightness temperatures for cloud-free pixels (Uesawa 2009). NWP centers will use the Himawari-8/9 CSR product in their operational assimilation systems as a primary data source. Data are calculated for each 16 × 16 infrared pixel box corresponding to approximately 32 × 32 km^2 resolution at the sub-satellite point for the global data assimilation system. The status of pixels as clear or cloudy is determined from the fundamental cloud product. In addition to the ordinary clear pixels provided from this product, cloudy pixels in which the contribution of cloud top emission to total radiance is negligible can also be regarded as clear for AHI bands with strong absorption (e.g., water vapor bands). These

Table 8. Evaluation of fundamental cloud product (prototype). (a) Accuracy of cloud mask for individual cloud types and phases, (b) accuracy of cloud mask for individual seasons and surfaces, (c) bias and standard deviation of cloud height for individual cloud types, and (d) definitions of accuracy and hit rate.

(a)

		Accuracy/hit rate
Mask (Ac.)		0.85
Type	Opaque (H.R.)	0.66
	Semi-transparent (H.R.)	0.80
Phase	Ice cloud (H.R.)	0.98
	Liquid water cloud (H.R.)	0.94

(b)

Mask		Accuracy				
		Winter	Spring	Summer	Autumn	All
All regions		0.86	0.85	0.85	0.85	0.85
Individual	Sea	0.86	0.85	0.85	0.86	0.85
	Snow/Ice	0.86	0.81	0.72	0.86	0.81
	Dessert	0.87	0.86	0.86	0.89	0.87
	Vegetation	0.86	0.84	0.83	0.83	0.84
	Others	0.80	0.82	0.86	0.84	0.84

(c)

Height	Bias (km)	Standard deviation (km)	Number
Low opaque	–0.1	1.34	2296940
High/mid opaque	0.31	1.33	1375505
Opaque	0.05	1.34	3672445
Semi-transparent (intercept or radiance rationing)	2.38	3.34	877586

(d)

		MODIS product detection	
		Yes	No
Fundamental cloud product detection	Yes	Correct detection (A)	False alarms (B)
	No	Misses (C)	Correct negatives (D)

A, B, C and D denote the number of occurrences for each case. Accuracy and hit rate are defined as below.
Accuracy = (A + D) / (A + B + C+ D)
Hit rate = A / (A + B)

CSR products are provided in Binary Universal Form for data Representation (BUFR) via the Global Telecommunication System (GTS).

6.3 AMV product

AMV is one of the most important meteorological satellite products in NWP. For example, Bormann et al. (2012) showed that AMVs from satellites have a positive impact on forecast skill in the ECMWF data assimilation system. JMA has developed a new algorithm for Himawari-8/9 AMVs (Shimoji 2014) based on an optimal estimation method for full exploitation

of satellite data. Improvement from the previous operational algorithm (Oyama 2010) results in the computation of wind vectors with high spatial resolution based on the tracking of smaller cloud patterns. Figure 10 shows a comparison of MTSAT observation data AMVs produced with the previous operational algorithm and the new algorithm for Himawari-8/9. Wind vectors with the new high-quality algorithm (Quality Indicator (QI) > 80) (Holmlund et al. 1998) are seen in the figure over wide areas where none are produced with the previous version. As with CSR, the AMV products are provided in BUFR via the GTS.

6.4 Volcanic ash product

Volcanic ash quantitative information (e.g., ash cloud height, optical depth, effective particle radius, and mass loading) from satellites is especially important in aviation usage. When Eyjafjallajökull erupted in 2010, Stohl et al. (2011) used volcanic ash information from satellites as initial values for their dispersion model. Frequent AHI multispectral observation is expected to help to improve this product. JMA has introduced two volcanic ash product retrieval algorithms for Himawari-8/9. One was provided by EUMETSAT (Prata 2011), and the other was provided by NOAA/NESDIS (Pavolonis and Sieglaff 2012). The EUMETSAT algorithm was modified by JMA, and its cloud height assignment data are provided to Tokyo VAAC (Tsuchiyama 2013). JMA is also currently developing a test bed for intercomparison of the volcanic ash retrieval algorithms. The test bed is built within the framework of the Sustained, Co-Ordinated Processing of Environmental satellite data for NoWCasting (SCOPE-NWC) Pilot Project for comparison of the EUMETSAT and NOAA/NESDIS algorithms. A case study involving volcanic ash from Mt. Kirishima on the Japanese island of Kyushu was conducted using MTSAT-2 observation data as shown in Fig. 11, where the ash cloud from the volcano is shown in red. Figure 12 shows the preliminary results of intercomparison for ash cloud height data obtained with the two algorithms. A marked difference in their spatial distributions is observed, especially in the southwestern area. Ash cloud height data from the NOAA/NESDIS algorithm are located at 0–6 km in the histogram, while those from EUMETSAT are located at 2–4 km. A scatter plot of the two data sets shows the same tendency. In this case, there is no data set such as ground-based lidar for validating which product is more accurate. Accordingly, further study is needed to clarify the reason for this difference.

6.5 Aeolian dust product

JMA monitors trends of Aeolian dust in light of the serious damage it causes to social activity, human health and economies in East Asia. Using Himawari-8/9 observation data, the Agency produces two aerosol products for Asian dust event monitoring. One of these, derived from visible and near-infrared data, provides daytime information on aerosol optical thickness and Angstrom index values (a metric of aerosol particle size) for areas over oceans and also provides aerosol optical thickness values for areas over land (Fig. 13). The algorithm involves the use of a look-up table calculated with the assumption of a spheroid-particle aerosol model (Okada et al. 2001). The other product provides quantitative information on dust using infrared data from Himawari-8/9. One of the advantages of the infrared dust product is its availability during both day and night time. The algorithm is based on that of the volcanic ash product for GOES-R developed by NOAA/NESDIS mentioned in the previous section, as the optical properties of dust are similar to those of volcanic ash. In addition to these two algorithms, the development of a further algorithm is under discussion with aerosol scientists in Japan for aerosol data assimilation. JMA will use these new aerosol products based on Himawari-8/9 observation data in the future.

6.6 Rapidly Developing Cumulus Area product

Himawari-8/9 make observations over Japan at 2.5-min intervals. The advent of frequent observations from space is expected to help to improve severe weather analysis and forecasting. The Rapidly Developing Cumulus Area (RDCA) product has been developed to support the monitoring of rapidly developing convective cloud based on rapid-scan (5-min interval) observations made by MTSAT-1R around Japan during the daytime (00 to 09 UTC) in summer (June to September) (Sumida et al. 2015). The RDCA product highlights areas at high risk of active convection and heavy rainfall. Its algorithm detects rapid changes in cloud conditions (e.g., sudden genesis and evolution of cumulonimbus cloud) based on a statistical approach by matching up satellite observation with ground-based lightning remote sensing observation. Figure 14 shows an example of RDCA information retrieved from MTSAT-1R observation data at 08:45 UTC on 11 July 2011. The green region shows a rapidly developing cumulus area, and the red region shows a cumulonimbus area. These areas correspond closely to the severe convective region estimated from ground-based remote sensing results (i.e.,

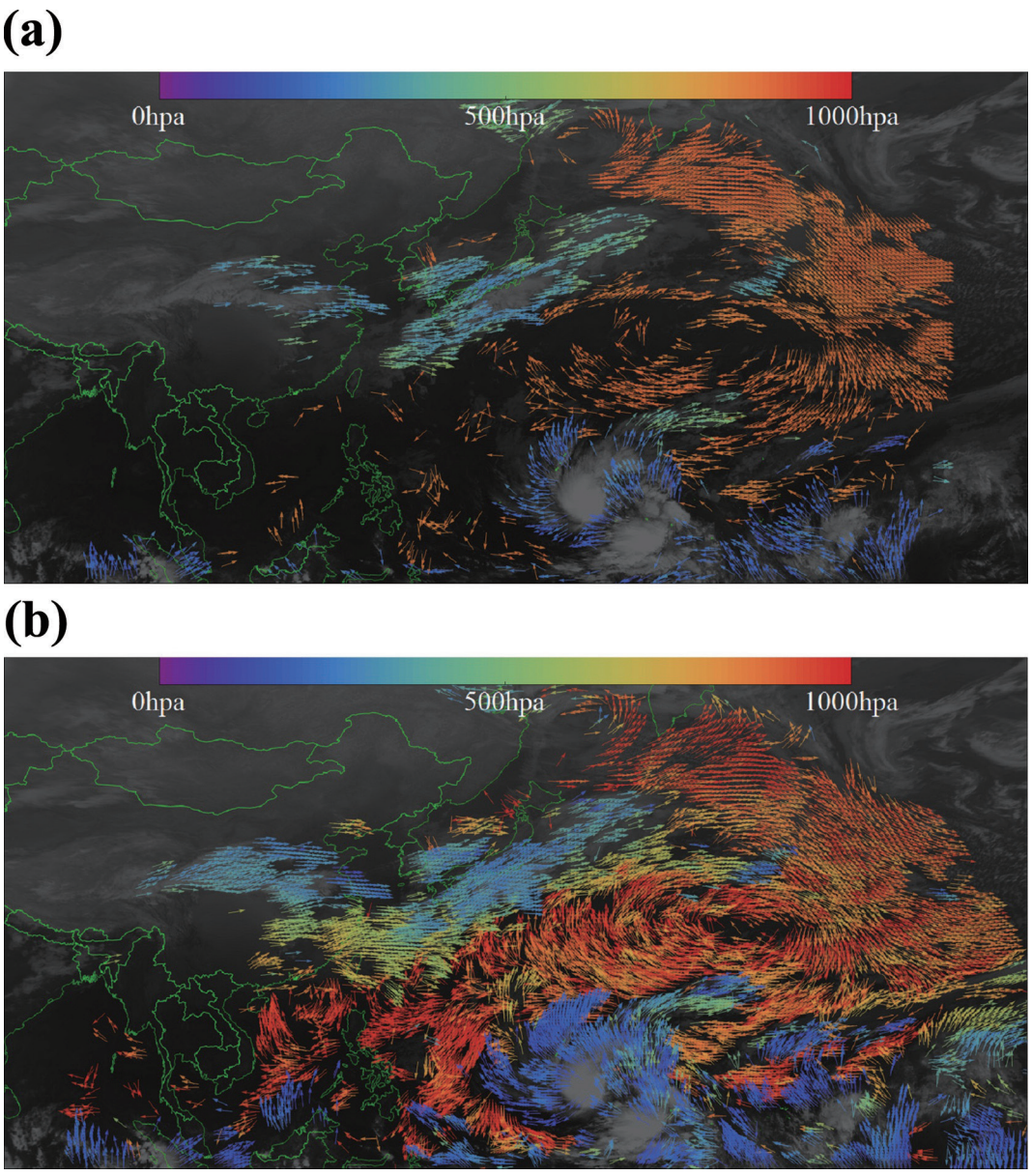

Fig. 10. MTSAT IR wind vectors (QI > 80) retrieved using the previous operational algorithm (a) and with the newly developed algorithm for Himawari-8/9 (b) at 00 UTC on 2 March 2014. Warm colors correspond to low-level wind and cold colors to high-level wind.

those from radars and lightning detection networks in Japan). The product's algorithm will be modified using Japan Area observation data observed every 2.5 min by Himawari-8/9. After this improvement, the RDCA product will be provided at all times during every season. As a further step, JMA has started planning the development of global RDCA product using Himawari-8/9 Full Disk observation data obtained every 10 min. This product will contribute to safety and control of air traffic over the East Asia and Western Pacific regions.

6.7 RGB composite image product

As Himawari-8/9 have 16 bands that can be combined in a large number of ways, it will be difficult for forecasters and analysts to digest combined

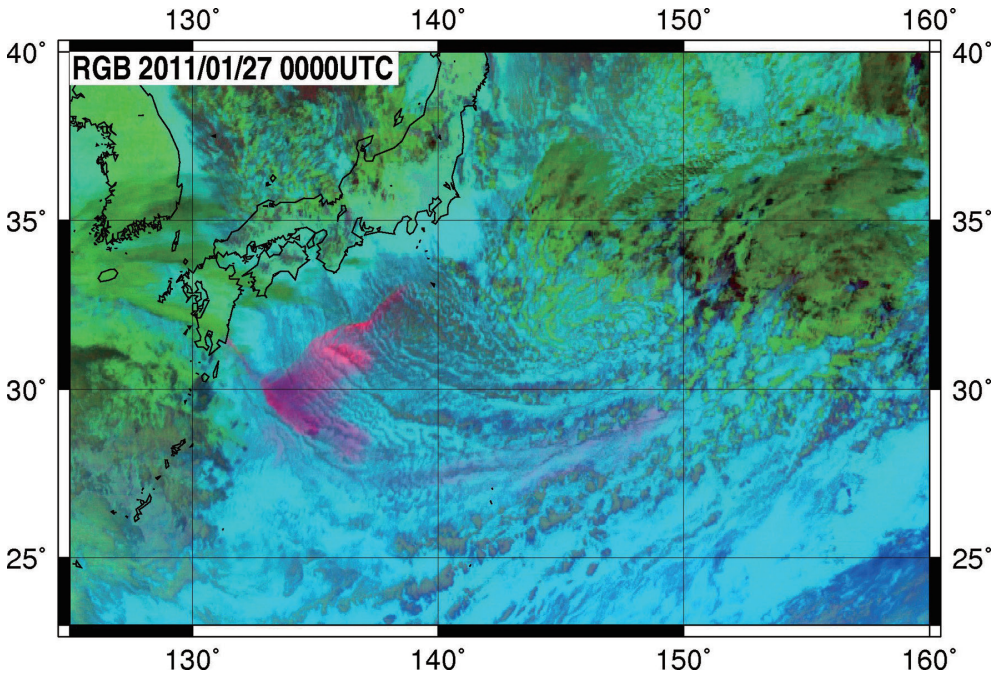

Fig. 11. RGB composite image from MTSAT-2 at 00 UTC 27 January 2011. RGB are defined (red: IR10.8–IR12.0; green: IR3.9–IR10.8; blue: IR10.8) to enhance volcanic ash presence (Pavolonis 2013, personal communication).

AHI imagery at a glance. Accordingly, there is a need for the satellite operator to provide satellite images that can be easily interrupted. Red, green, and blue (RGB) composite images support this purpose. Imagery from Himawari-8/9 AHI is provided by JMA for NMHSs in Southeast Asia and the South Pacific islands via the MSC website in the combinations recommended at the RGB Composite Satellite Imagery Workshop, which are based on observation results for MSG/SEVIRI with 12 bands (WMO and EUMETSAT 2007). As with the MTSAT RGB composite images on the MSC website, Himawari-8/9 RGB images will contribute to the WMO Commission for Basic Systems (CBS) Severe Weather Forecasting Demonstration Project (SWFDP) and the Severe Weather Forecasting and Disaster Risk Reduction Demonstration Project (SWFDDP) (Fig. 15).

6.8 Contribution to ISCCP and GPCP

The International Satellite Cloud Climatology Project (ISCCP) was established to collect and analyze weather satellite radiance data that would help to clarify the global distribution, properties, and temporal variation of clouds. Its datasets and analysis products are used to study how clouds affect climatic characteristics. The purpose of the Global Precipitation Climatology Project (GPCP) is to help clarify spatial and temporal patterns of global precipitation. Data from rain gauge stations, geostationary/low-earth-orbit satellites, and sounding observation work are merged to enable the formulation of monthly rainfall grid maps. JMA has contributed to the ISCCP since data collection started in July 1983 and to the GPCP since its establishment in 1986. The Agency processes observation data from eight geostationary satellites (including GMS, the MTSAT series, and GOES-9) and provides the outcomes to ISCCP and GPCP processing centers on a routine basis. The resulting ISCCP and GPCP products improve understanding and modeling of the climate and support cloud studies, including clarification of the hydrological cycle. JMA will continue to support both projects after the start of Himawari-8/9 operation.

6.9 Contribution to SCOPE-CM

SCOPE-CM is envisioned as a component of a framework linking satellite observation technology such as GOS with inter-calibration technology such as GSICS to provide required climate data records addressing the Essential Climate Variables (ECVs) (Lattanzio et al. 2013). JMA computes AMVs, CSR, and land surface albedo data from the observations of

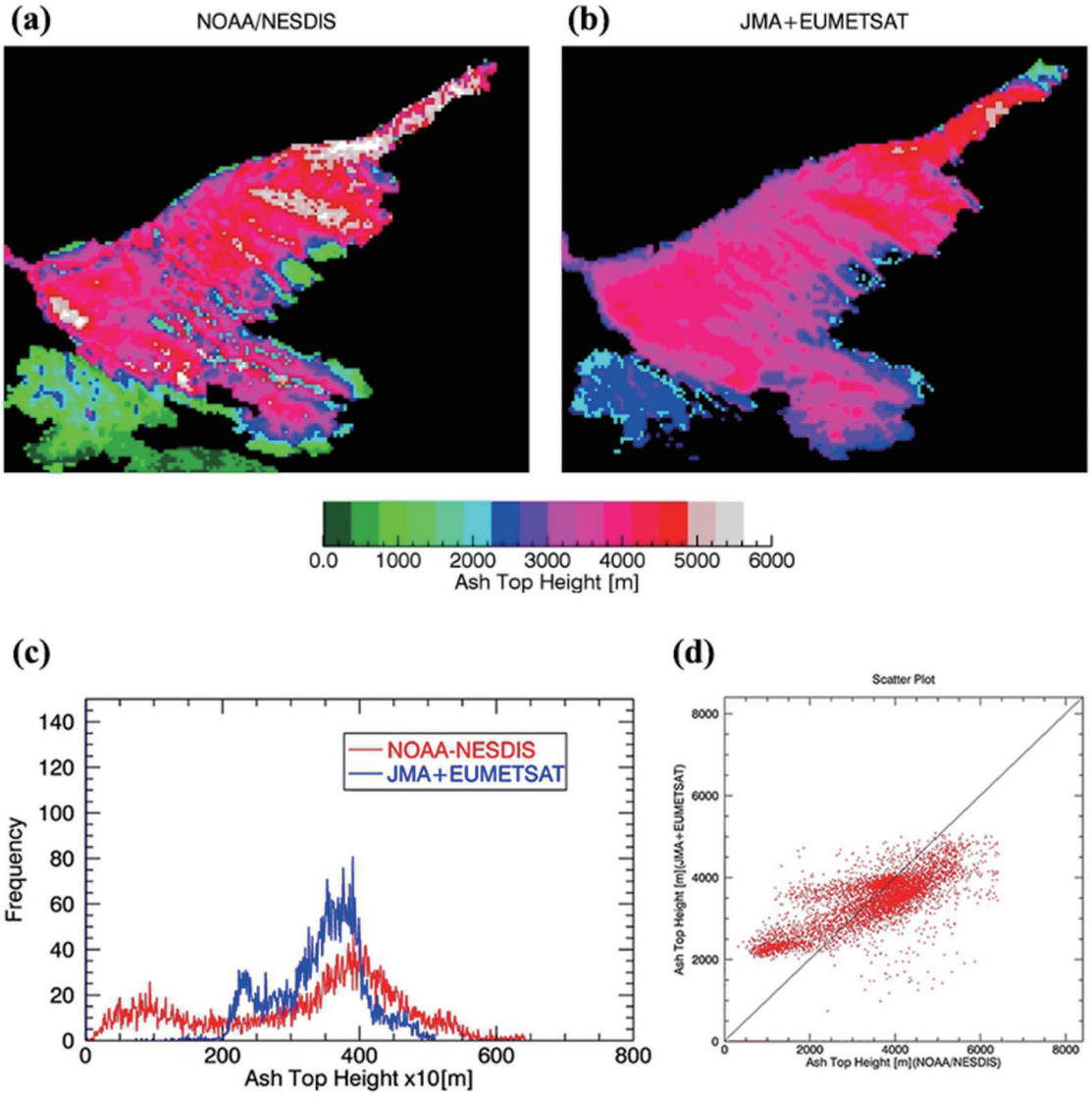

Fig. 12. Volcanic ash cloud height retrieval intercomparison between the NOAA/NESDIS and EUMETSAT algorithms for Mt. Kirishima at 00 UTC on 27 January 2011. The graphs show spatial distribution of height (a and b), histograms (c), and a scatter plot representation (d).

past satellites and provides the results to SCOPE-CM. AMVs and CSR products are also provided to the European Centre for Medium-Range Weather Forecasts (ECMWF) Re-Analysis (ERA) Interim Project (Dee et al. 2011) and the Japanese 55-year Re-Analysis (JRA-55) Project (Kobayashi et al. 2015) for contribution to climate research fields. Himawari-8/9 are capable of performing Full Disk observation every 10 min. JMA's development of a new AMVs retrieval method for the satellites as outlined above is expected to represent an ongoing contribution to long-term climate research.

7. Future plans

The previous section outlined basic physical products retrieved from Himawari-8/9 observation data by JMA. Each product has its own improvements over the previous ones developed for MTSAT series data. However, there is still plenty of scope to improve existing or develop new physical products or satellite applications using observation data from Himawari-8/9. As already detailed, Himawari-8/9

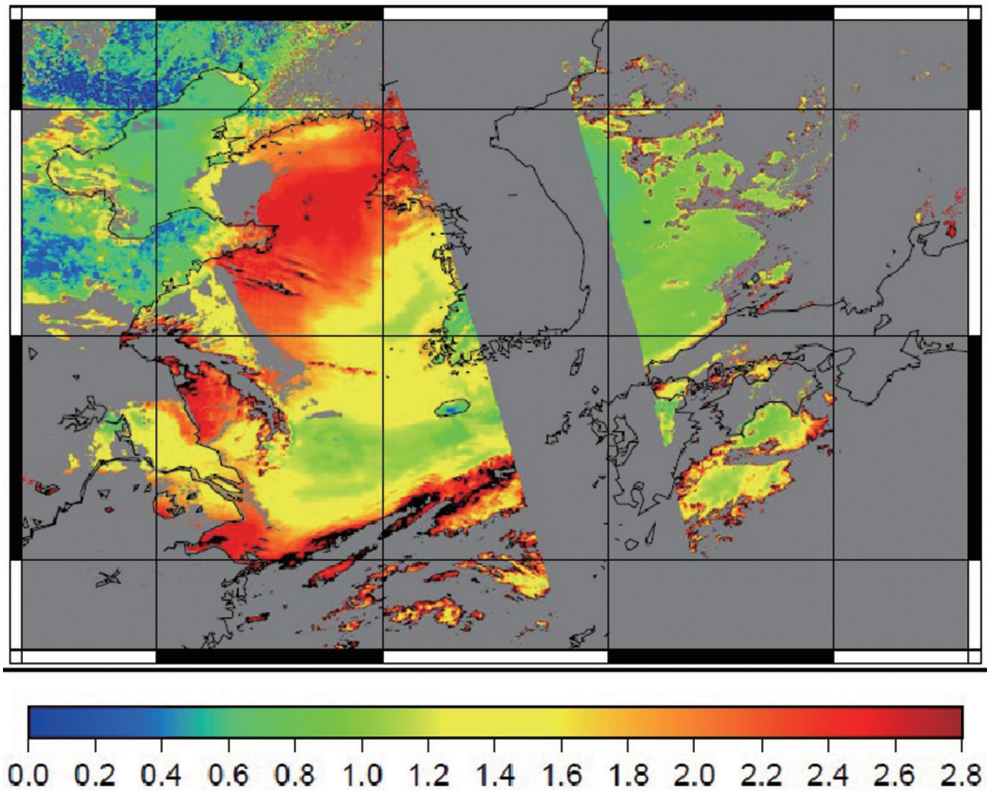

Fig. 13. Prototype aerosol optical thickness product without cloud mask derived using the algorithm for Himawari-8/9 made using data from NASA's Terra/MODIS satellite with bands corresponding to those of AHI/Himawari-8/9.

have huge capability in terms of temporal and spatial high-resolution observation with 16 bands. To fully utilize the data, it is necessary to keep some key concepts in mind such as conjunction with numerical models, advanced data assimilation, application to frontier themes, and combination of multi-observation platforms. As no operator has yet handled data sets from new-generation geostationary meteorological satellites, innovative ideas based on these concepts are needed to bridge the gap between observation data supply and usage.

Until now, data from low-earth-orbit environmental satellites and meteorological polar-orbiting satellites with visible/infrared imagers have helped to reveal major characteristics of cloud, especially in climatology, through the use of a variety of physical product retrieval algorithms (e.g., Remer et al. 2005). Application of this knowledge to observation results from the 16 AHI bands is expected to offer new insights into cloud climatology. By way of example, information showing cloud properties such as optical thickness, particle size, thermo-dynamical phase, and cloud top temperature from AHI observation data are considered important in climatological cloud database development. Other environmental parameters retrieved from Himawari-8/9 AHIs are also viewed as indispensable for their coverage of wide areas and long time periods in the fields of hydrology, glaciology, oceanography, and ecology.

In addition to their advantage of having more spectral bands, the AHIs feature faster imaging and higher spatial resolution than MTSAT/Imager. The detailed cloud information inferred from Full Disk images taken every 10 min and Japan-area images taken every 2.5 min by the AHIs shows the lifecycle of cloud, including its genesis, evolution, and decay, more clearly than ever before. By way of example, Nakajima et al. (2010a, b) suggested that temporal variations in cloud evolution could be clarified using observation results from AHI bands #5–7, which belong to the near-infrared or infrared wavelength. Cloud droplet size can also be estimated from differ-

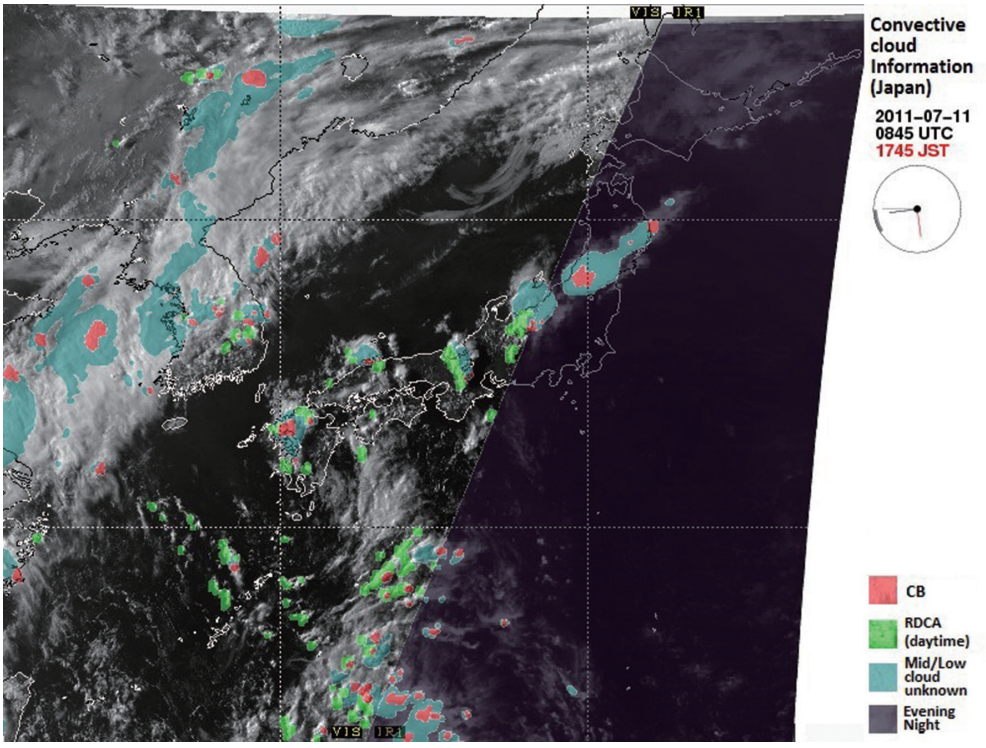

Fig. 14. RDCA product imagery at 08:45 UTC on 11 July 2011. RDCAs are shown in green, cumulonimbus in red, and unknown areas covered by mid- or low-level cloud in aqua. The nighttime area where the solar zenith angle exceeds 75° is shown in purple; no RDCAs are seen in the nighttime area.

ences in the effective vertical weighting function between these bands. Traditional radar meteorology, which involves scientific study of the atmosphere using radar observation results, can be seen as a type of mesoscale rain meteorology. The AHI units on board Himawari-8/9 will open the door to a new era of mesoscale cloud meteorology. In other words, mesoscale satellite meteorology will be born from these new-generation geostationary meteorological satellites. The next step in this satellite revolution will involve a new research theme dealing with a range of matters from cloud particle genesis to rainfall decay in an integrated manner with a combination of radar and satellite observations.

JMA plans to help mitigate the effects of natural disasters and resolve global environmental problems by maximizing the observational ability of Himawari-8/9. To this end, the Agency established an application technology advisory panel in 2009 for next-generation geostationary meteorological satellites. The panel consists of professors and researchers from Japanese universities and Japan Aerospace Exploration Agency (JAXA) and is tasked with discussing the needs of satellite data users, the direction of research and development in satellite usage, and the promotion of satellite data utilization. In 2014, two working groups were organized under the panel to exploit techniques for Himawari-8/9 data application in science relating to the atmosphere and oceans/land. JMA pursues the development of new physical products from Himawari-8/9 in collaboration with the scientific community in Japan as outlined previously. This section covers future products from the new-generation of geostationary satellites and related applications based on the key concepts detailed above.

7.1 Optimal Cloud Analysis

To exploit the full potential of AHI multispectral observations, Optimal Cloud Analysis (OCA) (Watts et al. 2011) will be introduced in collaboration with EUMETSAT. OCA involves use of the optimal estimation method (1D-Var) for the simultaneous retrieval of cloud and surface parameters (e.g., cloud optical thickness, cloud effective radius, cloud top

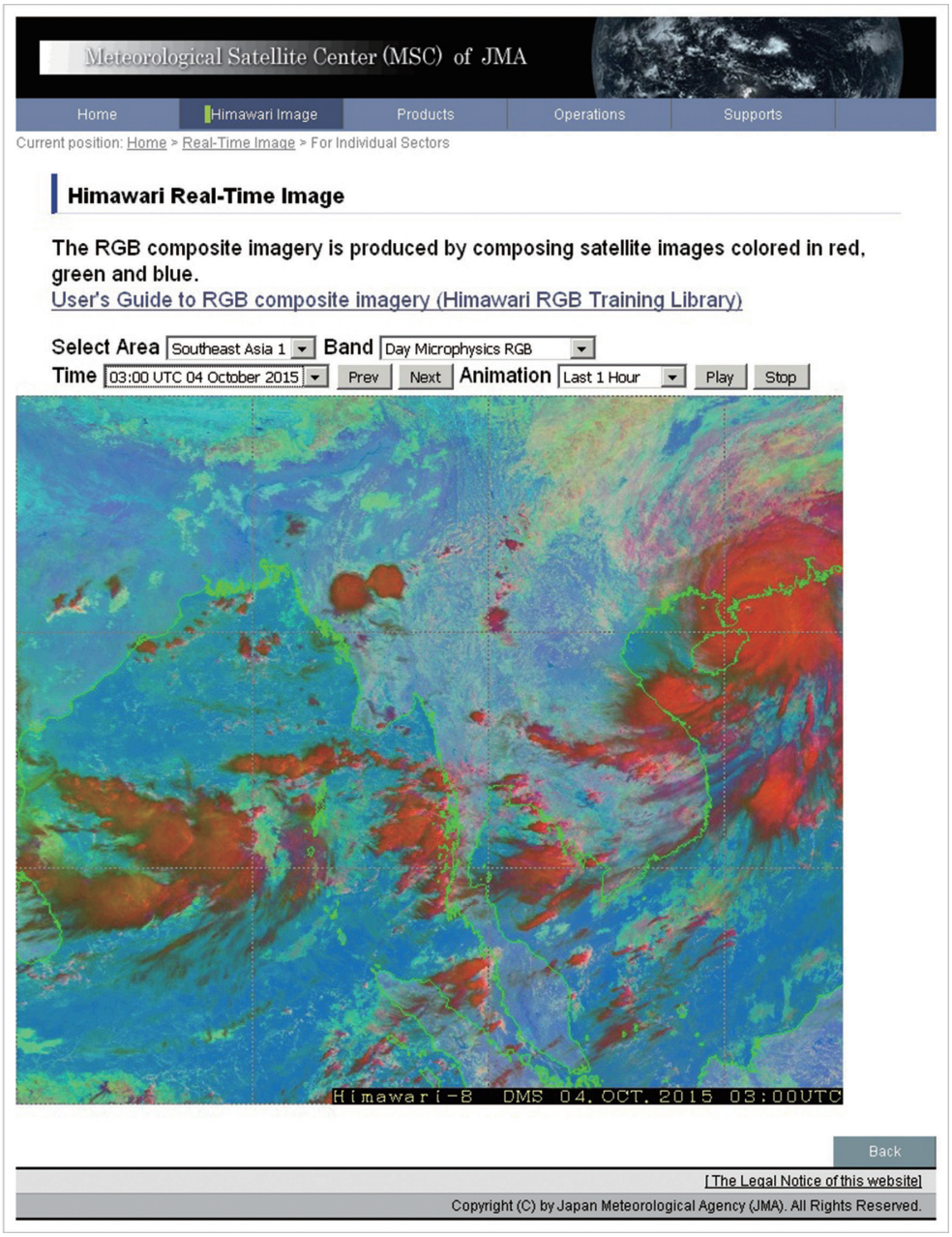

Fig. 15. MSC website for provision of RGB composite images from Himawari-8 to users of SWFDP and SWFDDP of WMO/CBS. [Available at http://www.data.jma.go.jp/mscweb/data/himawari/index.html.]

pressure, and surface temperature). Cloud microphysical parameters (e.g., effective radius) estimated from Himawari-8/9 AHI observations with high temporal resolution (an interval of 2.5 min around Japan) have the potential to provide information on cloud genesis, evolution, and decay. JMA has run OCA with SEVIRI data as a proxy for AHI data. Figure 16 compares cloud height data retrieved from OCA with reference data such as satellite Cloud-Aerosol Lidar and Infrared Pathfinder Satellite Observation (CALIPSO) products. A high level of consistency in the cloud height is observed from this figure.

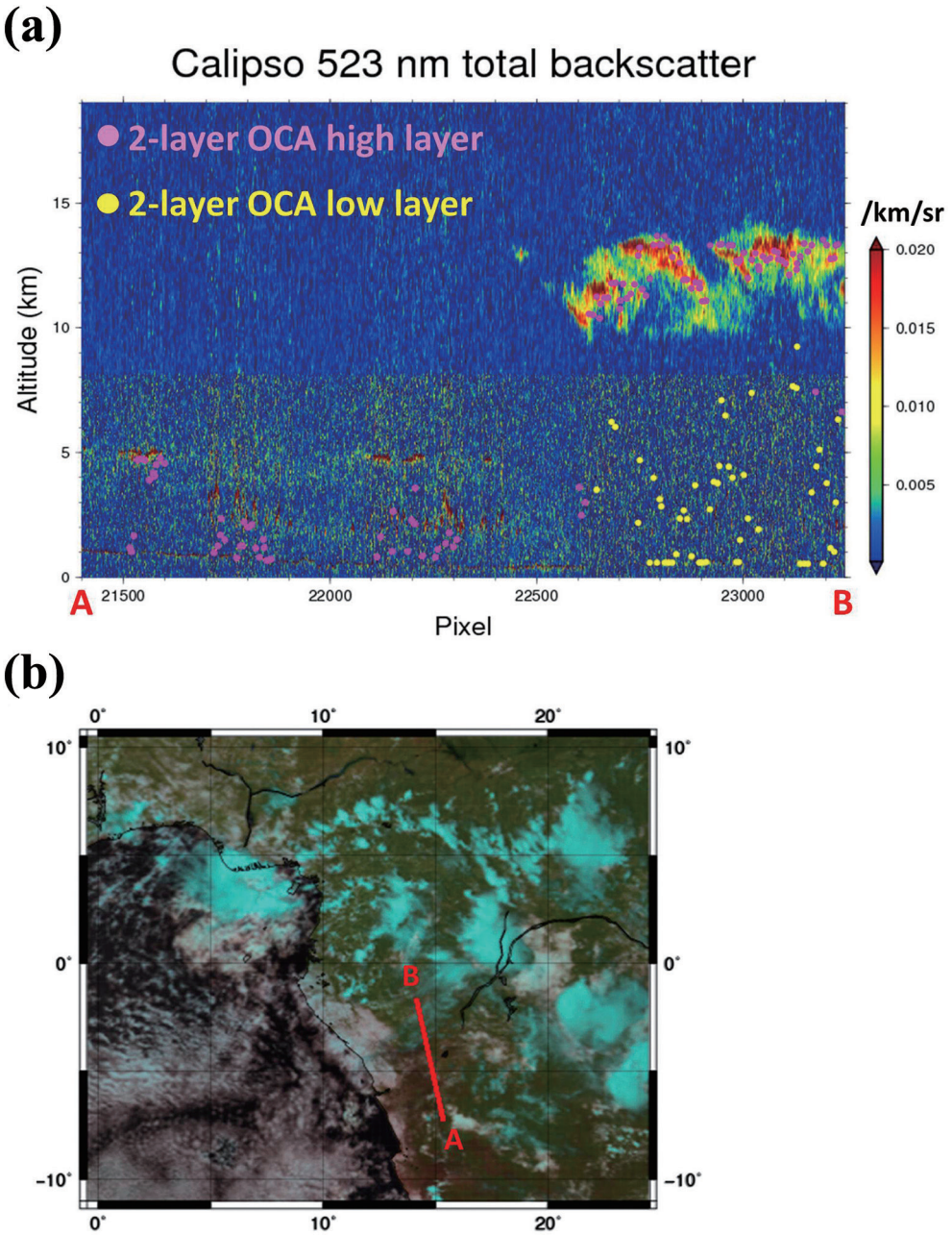

Fig. 16. Comparison between OCA cloud height data retrieved from SEVIRI and Cloud-Aerosol Lidar with Orthogonal Polarization (CALIOP) data at 13 UTC on 1 October 2013 over Central Africa. (a) shows the height/path cross section of CALIOP 523 nm total attenuated backscatter coefficients along a path (A–B) of CALIPSO. High-layer cloud heights (purple circles) and low-layer cloud heights (yellow circles) estimated using OCA are superimposed onto the cross section. (b) shows a SEVIRI RGB composite image (red: 1.64 μm; green: 0.81 μm; blue: 0.64 μm). The red line from A to B corresponds to the path of CALIPSO shown in (a).

7.2 Atmospheric stability index product

JMA plans to produce a stability index product for cloud-free conditions. This will be similar to the Legacy Atmospheric Profile (LAP) product for GOES-R developed by NOAA/NESDIS (Lee et al. 2014) and the Global Instability Index (GII) for MSG

developed by EUMETSAT (Koenig and Coning 2009). The product will provide atmospheric stability indices such as Convective Available Potential Energy (CAPE), K-Index, and precipitable water values. The algorithm will involve the use of an optimal estimation method (e.g., 1D-Var) so that multispectral AHI information can be fully used to retrieve atmospheric profiles and calculate stability indices. The product will support weather forecasters by enabling early detection of severe weather phenomena such as thunderstorms.

7.3 Advanced convective cloud detection product

JMA is currently developing a more advanced convective cloud retrieval product using the JMA Non-Hydrostatic Model (JMA-NHM) (Saito et al. 2006) and the RSTAR radiative transfer model. The evolution of local heavy rainfall is simulated using JMA-NHM, and successive satellite images are then created at short time intervals by RSTAR as the satellite simulator. The use of a numerical model and a satellite simulator can provide deep insights into the relationship between physical parameters and their radiative signatures for convective cloud. If new information is found in this regard, data from Himawari-8/9 may provide absolute evidence of rapid convection. The combination of Himawari-8/9 data and other observation data from radars, the lightning detection network, wind profilers, and upper soundings is expected to improve the accuracy of nowcasting for severe weather phenomena such as localized heavy rain, thunderstorms, and tornadoes.

7.4 AMVs for Nowcasting

AMVs derived from short-interval images are considered useful for capturing short-lived phenomena such as rapidly developing cumulus cloud or rapidly deforming typhoon cloud systems. Advanced SCATterometer (ASCAT) surface wind data are currently utilized as a major ancillary resource in JMA's typhoon analysis and, in particular, for the estimation of gale force wind areas over data-sparse sea regions. However, as ASCAT coverage is temporally sparse (the ASCAT units on board Metop satellites observe the same points twice a day), data-sparse regions need to be compensated for by other observations. As mentioned in Section 6, MTSAT-1R performed special rapid-scan (5-min interval) observations around Japan during the daytime in summer. Figure 17 shows an example of comparison between MTSAT-2 hourly AMVs and MTSAT-1R Rapid-Scan AMVs obtained every 5 min (RS-AMVs) based on visible images in the vicinity of a typhoon. The number of RS-AMVs is clearly larger. The ability of rapid-scan images to capture short-lived cloud systems within typhoons supports their use for such compensation in data-sparse areas around typhoons. JMA also conducted a study to compare ASCAT wind and AMVs from rapid-scan visible imagery covering the vicinity of a typhoon to validate the use of RS-AMVs in typhoon analysis. Figure 18 shows the results of a comparison between RS-AMVs from visible imagery and ASCAT wind data from around the vicinity of 2011's Typhoon Ma-on. Wind speed comparison shows close correspondence, but the mean speed of ASCAT winds is about 0.8 times that of RS-AMVs up to 15 m s^{-1}. Wind direction differences are small compared to speed differences, but ASCAT winds are directed about 10° inward to the typhoon center with RS-AMVs as a reference. These results indicate a close correlation between sea-surface winds and AMVs, as suggested by previous work involving the use of sea-surface wind data from in-situ observations (e.g., Ohshima et al. 1991; Dunion and Velden 2002). Meanwhile, the wind speed of RS-AMVs is greater than that of ASCAT winds in the high-speed region. This bias requires further investigation. AMVs provided by Himawari-8/9 on the basis of observations made every 10 or 2.5 min are expected to be similar to MTSAT-1R RS-AMVs.

7.5 Analysis of upper-tropospheric flows in typhoon using AMVs

Using rapid-scan imageries from geostationary satellites obtained at intervals of less than 10 min, tracking the clouds is enabled in typhoons where the direction of cloud motion abruptly changes and active convections occur. The upper-tropospheric AMVs, which were retrieved from the tracks of upper-tropospheric clouds or water vapor patterns from MTSAT-1R rapid-scan imageries, were applied to analysis of wind field in typhoons. The analyses of several typhoons revealed that both tangential and radial wind components of the AMVs, which correspond to cyclonic circulation and horizontal divergence in the upper troposphere near the typhoon center, increased in the rapid intensification stage of the typhoons. This result indicates that the AMVs reflected the intensification of the primary and secondary circulations of the typhoons during their intensification. It is expected that studies using upper-tropospheric AMVs from Himawari-8/9 for typhoons will contribute to an understanding of

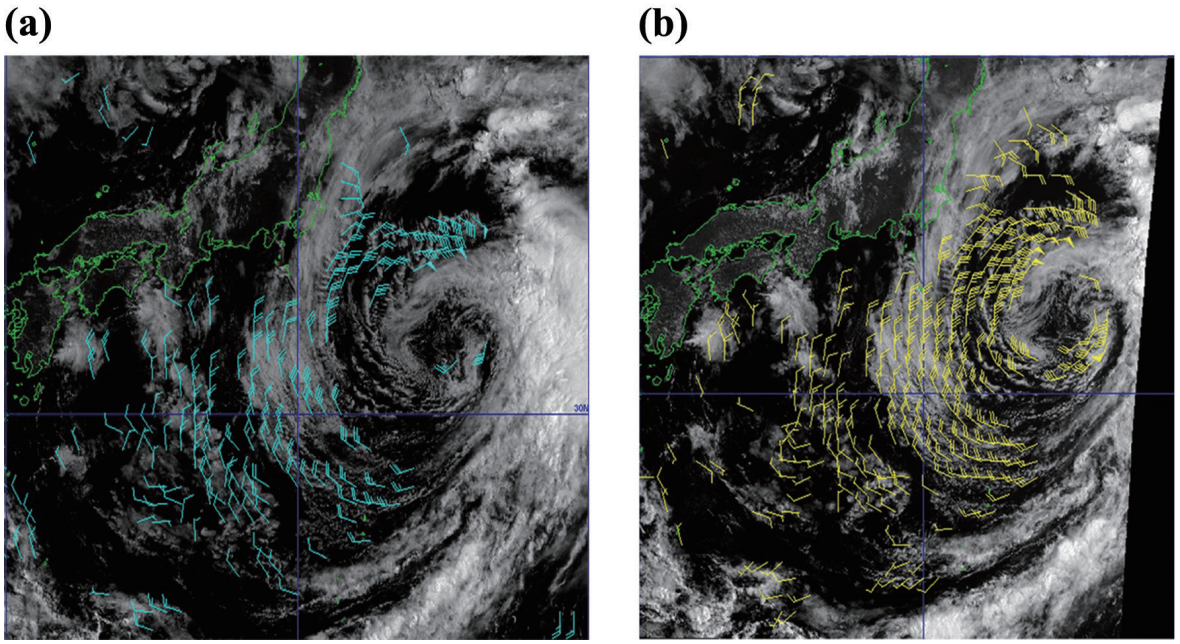

Fig. 17. MTSAT-2 hourly AMVs (a, blue barbs) and MTSAT-1R rapid-scan AMVs (b, yellow barbs) based on visible images in the vicinity of Typhoon Ma-on at 00 UTC on 23 July 2011

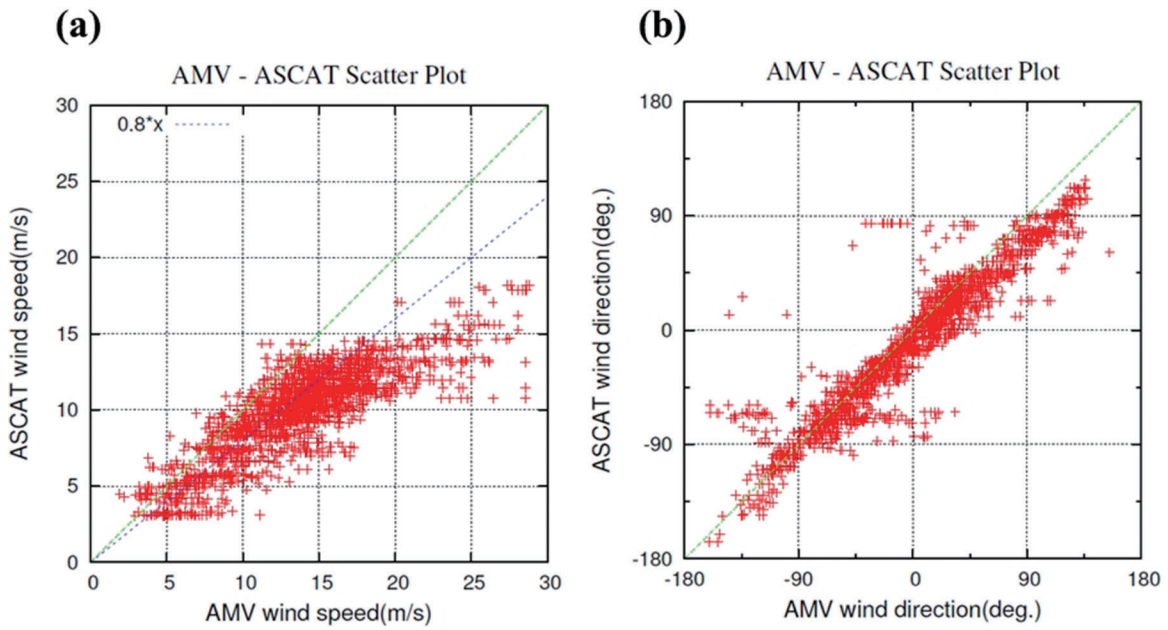

Fig. 18. Scatter plots of MTSAT-1R rapid scan wind from visible imagery and ASCAT wind data. (a) shows wind speed, and (b) shows wind direction. The comparison period is from 17 to 23 July 2011, which is approximately when Typhoon Ma-on was within MTSAT-1R's rapid-scan area.

typhoon intensification processes and the diagnosis of typhoon intensity change.

7.6 Solar radiation estimation for photovoltaic power

Expectations for the widespread utilization of renewable energy forms such as photovoltaic power have been high in recent years, especially since the Great East Japan Earthquake of 2011. Photovoltaic power has significant potential to contribute to Japan's electric power supply, but is usually subject to variations in solar radiation. Accordingly, the ability to estimate and predict solar radiation accurately is of great importance. Geostationary meteorological satellites are useful tools in this regard because they are used to observe large areas of the earth with high temporal frequency and moderate spatial resolution. In this area, Takenaka et al. (2011) developed a new algorithm for solar radiation estimation from MTSAT-1R observation data using a neural network based on radiative transfer in near-real-time. In this system, cloud properties are retrieved from the Comprehensive Analysis Program for Cloud Optical Measurement (CAPCOM) (Nakajima and Nakajima 1995; Kawamoto et al. 2001). Plans are currently being made to apply the huge observational ability of Himawari-8/9, which have high temporal frequency, high spatial resolution, and 16 bands, to the precise estimation of solar radiation.

7.7 Super-rapid assimilation for super-rapid scan data from Himawari-8/9

Heavy rainfall concentrated in very small areas has caused major disasters in Japan in recent years. Such localized downpours are usually brought by convective clouds whose typical lifecycle is less than an hour. In 2013, Japan's RIKEN Advanced Institute for Computational Science began using the Japanese 10-petaflop K computer in its Big Data Assimilation science program for super-rapid 30-s cycles of an ensemble Kalman filter to forecast such local severe weather at a 100-m resolution with a 30-min lead time. This forecast system is 120 times more rapid than the current hourly updated ones and will help prepare for sudden local torrential rainfalls that may cause flash flood and river outflow only within 10–20 min. In this work, observational data from Landmark Areas obtained every 30 s by Himawari-8 will also be assimilated with other sub-minute observation data such as phased array weather radar information. These data may be frequent enough to capture the nearly linear evolution of convection. As the volume of data from these new observing platforms will be two orders of magnitude greater than before, the effective use of such big data in very-short-range NWP is a big challenge and may only be possible with a 10-petaflop system such as the K computer.

7.8 Targeted observation

As detailed in Section 4, the AHI imager units on board Himawari-8/9 have the capability for flexible observation of the Target Area every 2.5 min and Landmark Areas every 30 s to enable targeted monitoring. Such targeted observation is an enhancement of the operational observation network to be assimilated into NWP. Additional observations will be performed in sensitive regions as estimated from ensemble forecasts, where these additional observation data will be effective in improving prediction results. These approaches have been implemented in a variety of field experiments, including The Observing System Research and Predictability Experiment (THORPEX) (Majumder et al. 2011), of which the THORPEX-Pacific Asian Regional Campaign (T-PARC) was a sub-program. JMA began contributing to this experiment in 2008 and executed special observations such as dropsonde observation in collaboration with Germany's Falcon research aircraft, enhanced upper sounding using two research vessels and four automatic upper-sounding stations, and MTSAT-2 rapid-scan operations (Nakazawa et al. 2010). The effectiveness of assimilating AMVs from MTSAT-2 rapid scan observation data in T-PARC for NWP was validated by Yamashita (2010) and Wu et al. (2014). Flexible observation by Himawari-8/9 offers significant opportunities for operational targeted observation. As a first step, experimental application of these AHI functions is expected with sensitivity analysis based on ensemble prediction toward the goal of NWP innovation.

8. Conclusions

As described in this paper, new-generation geostationary satellite platforms such as Himawari-8/9 carry optical sensors with significantly higher radiometric, spectral, and spatial resolution than those previously available in geostationary orbit. These advantages, when combined with fast revisit times of 10 min or less, will provide revolutions of capability for the identification and tracking of rapidly changing weather phenomena. They will also support the development of new surface and atmospheric monitoring/mapping applications in which high temporal frequency and near real-time image

supply are essential. From another point of view, the data set of AHI, which is the first 16 bands imager in geostationary orbit, serves as test data for the applications ground segment of other new-generation satellite imagers such as GOES-R/ABI, GEOstationary KOrea Multi-Purpose SATellite-2A (GEO-KOMPSAT-2A)/Advanced Meteorological Imager (AMI), MTG/Flexible Combined Imager (FCI), and so on. JMA processes raw data from Himawari-8/9 with quality control and creates HSD, imagery, and physical products for its own use in NWP, severe-weather watching, and environmental monitoring. The Agency also provides Level-1b data to external users via multiple channels including the Himawari-Cloud service and the HimawariCast service.

Himawari-8/9 provides Full Disk observation data every 10 min by default. As such high-frequency Full Disk scanning is expected to become a world standard for emergency support in the near future, there is a need to develop and popularize the usage of high-frequency data for disaster risk reduction in collaboration with RSMCs and VAACs. It is also important to promote Himawari-8/9 data utilization in the East Asia and Western Pacific regions within the framework of CGMS. Wide-ranging application in various aspects of meteorological, hydrological, and climate operation by countries in these areas is expected to create a variety of new problems that will need to be addressed for more effective usage of Himawari-8/9 data. In this regard, JMA remains committed to its ongoing global contribution as a satellite operator and an NMHS.

There is significant potential for the application of Himawari-8/9 data to various areas outside the meteorological field, such as in other earth science fields and ecological/economic fields. To extract fruitful results from these data, JMA is dedicated to its role in joint work with operators in the science community. Collaborative research agreements on satellite data quality control and application have already been established between universities in Japan and JMA. Another example is JMA's engagement in collaboration on joint international development toward the creation of common scientific software for seamless determination of weather parameters by all meteorological satellite operators. JMA will continue these domestic and international collaboration efforts in order to further develop satellite data applications.

Supplement

Supplement 1 shows infrared (IR1 or band #13) animations from MTSAT-2 Northern Hemisphere images every 30 min (left) and Himawari-8 Japan Area images every 2.5 min at 11:00–19:30 UTC on 26 January 2015.

Acknowledgments

This paper has benefited from the contributions of numerous JMA staff. The authors thank everybody involved for their contribution. Thanks also go to the members of JMA's Advisory Panel on Application Technology for Next-generation Geostationary Meteorological Satellites and related working groups. Dr. Teruyuki Nakajima, who is a head of JAXA/Earth Observation Research Center (EORC), deserves special thanks for his leadership as chairman of the advisory panel. Appreciation is also due to Prof. Eiichi Nakakita of Kyoto University and Associate Prof. Hirohiko Masunaga of Nagoya University for their fruitful input in discussions on collaborative research. The authors would also like to thank Prof. Takashi Y. Nakajima of Tokai University (Principal Investigator in CREST/TEEDDA) and Dr. Takemasa Miyoshi of RIKEN AICS (Principal Investigator in CREST/BDA) for sharing their insights. Thanks also go to the Open Clustered Libraries for Atmospheric Science and Transfer of Radiation (OpenCLASTR) project for allowing the use of RSTAR package radiative transfer code in this research.

Appendix: List of acronyms

ABI	Advanced Baseline Imager
ACC	ACCelerometer
AHI	Advanced Himawari Imager
AIRS	Atmospheric InfraRed Sounder
AMI	Advanced Meteorological Imager
AMV	Atmospheric Motion Vector
AORI	Atmosphere and Ocean Research Institute
ARS	Angular Rate Sensor
ASCAT	Advanced SCATterometer
BUFR	Binary Universal Form for data Representation
CALIOP	Cloud-Aerosol Lidar with Orthogonal Polarization
CALIPSO	Cloud-Aerosol Lidar and Infrared Pathfinder Satellite Observation
CAPCOM	Comprehensive Analysis Program for Cloud Optical Measurement
CAPE	Convective Available Potential Energy
CBS	Commission for Basic Systems
CGMS	Coordination Group for Meteorological Satellites

CSR	Clear Sky Radiance
DCP	Data Collection Platform
DCS	Data Collection System
DVB-S2	Digital Video Broadcasting-Satellite-Second Generation
ECMWF	European Centre for Medium-Range Weather Forecasts
ECV	Essential Climate Variable
EMU	Environmental Monitoring Unit
EORC	Earth Observation Research Center
ERA	ECMWF Re-Analysis
EUMETSAT	EUropean organisation for the exploitation of METeorological SATellites
FCI	Flexible Combined Imager
GARP	Global Atmospheric Research Program
GII	Global Instability Index
GISC	Global Information System Centre
GMS	Geostationary Meteorological Satellite
GOES	Geostationary Operational Environmental Satellite
GEO-KOMPSAT-2A	GEOstationary KOrea Multi-Purpose SATellite-2A
GOS	Global Observing System
GPCP	Global Precipitation Climatology Project
GSICS	Global Space-based Inter-Calibration System
GSM	Global Spectral Model
GTS	Global Telecommunication System
HOPE	Himawari OPeration Enterprise corporation
HRIT	High Rate Information Transmission
HSD	Himawari Standard Data
HSF	Himawari Standard Format
IASI	Infrared Atmospheric Sounding Interferometer
ICSU	International Council of Scientific Unions
ICT	Internal Calibration Target
INR	Image Navigation and Registration
IR	InfraRed
IRU	Inertia Reference Unit
ISCCP	International Satellite Cloud Climatology Project
JAXA	Japan Aerospace Exploration Agency
JDDS	JMA Data Dissemination System
JMA	Japan Meteorological Agency
JPEG	Joint Photographic Experts Group
JRA-55	Japanese 55-year Re-Analysis
LAP	Legacy Atmospheric Profile
LNB	Low Noise Block converter
LOS	Line Of Sight
LRIT	Low Rate Information Transmission
MBCC	Midnight Blackbody Calibration Correction
MODIS	MODerate resolution Imaging Spectroradiometer
MSC	Meteorological Satellite Center
MSG	Meteosat Second Generation
MTG	Meteosat Third Generation
MTSAT	Multi-functional Transport SATellite
NASA	National Aeronautics and Space Administration
NESDIS	National Environmental Satellite, Data, and Information Service
NetCDF	Network Common Data Form
NHM	Non-Hydrostatic Model
NICT	National Institute of Information and Communications Technology
NIR	Near-InfraRed
NMHS	National Meteorological and Hydrological Service
NOAA	National Oceanic and Atmospheric Administration
NWP	Numerical Weather Prediction
OCA	Optimal Cloud Analysis
OpenCLASTR	Open Clustered Libraries for Atmospheric Science and Transfer of Radiation
PFI	Private Finance Initiative
PNG	Portable Network Graphics
QI	Quality Indicator
RDCA	Rapidly Developing Cumulus Area
RGB	Red, Green and Blue
RS	Rapid-Scan
RSMC	Regional Specialized Meteorological Centre
RSTAR	System for Transfer of Atmospheric Radiation
SATAID	SATellite Animation and Interactive Diagnosis
SCOPE-CM	Sustained, Co-Ordinated Processing of Environmental satellite data for Climate Monitoring
SCOPE-NWC	Sustained, Co-Ordinated Processing of Environmental satellite data for NoWCasting
SCT	Solar Calibration Target
SEDA	Space Environment Data Acquisition
SEVIRI	Spinning Enhanced Visible and Infrared Imager

SNR	Signal-Noise Ratio
SRF	Spectral Response Function
STT	STar Tracker
SWFDDP	Severe Weather Forecasting and Disaster risk reduction Demonstration Project
SWFDP	Severe Weather Forecasting Demonstration Project
THORPEX	The Observing System Research and Predictability Experiment
T-PARC	THORPEX - Pacific Asian Regional Campaign
VAAC	Volcanic Ash Advisory Center
VIS	VISible
WIS	WMO Information System
WMO	World Meteorological Organization
WWW	World Weather Watch

References

Bormann, N., K. Salonen, C. Peubey, T. McNally, and C. Lupu, 2012: An overview of the status of the operational assimilation of AMVs at ECMWF. *Proc. 11th Int. Winds Workshop*, Auckland, New Zealand, 20–24.

Dee, D. P., S. M. Uppala, A. J. Simmons, P. Berrisford, P. Poli, S. Kobayashi, U. Andrae, M. A. Balmaseda, G. Balsamo, P. Bauer, P. Bechtold, A. C. M. Beljaars, L. van de Berg, J. Bidlot, N. Bormann, C. Delsol, R. Dragani, M. Fuentes, A. J. Geer, L. Haimberger, S. B. Healy, H. Hersbach, E. V. Hólm, L. Isaksen, P. Kållberg, M. Köhler, M. Matricardi, A. P. McNally, B. M. Monge-Sanz, J.-J. Morcrette, B.-K. Park, C. Peubey, P. de Rosnay, C. Tavolato, J.-N. Thépaut, and F. Vitart, 2011: The ERA-Interim reanalysis: Configuration and performance of the data assimilation system. *Quart. J. Roy. Meteor. Soc.*, **137**, 553–597.

Dunion, J. P., and C. S. Velden, 2002: Application of surface-adjusted GOES low-level cloud-drift winds in the environment of Atlantic tropical cyclones. Part I: Methodology and validation. *Mon. Wea. Rev.*, **130**, 1333–1346.

Dvorak, V. F., 1975: Tropical cyclone intensity analysis and forecasting from satellite imagery. *Mon. Wea. Rev.*, **103**, 420–430.

Dvorak, V. F., 1984: *Tropical Cyclone Intensity Analysis Using Satellite Data*. NOAA Tech. Rep. NESDIS, **11**, US Department of Commerce, National Oceanic and Atmospheric Administration, National Environmental Satellite, Data, and Information Service, 47 pp.

Goldberg, M., G. Ohring, J. Butler, C. Cao, R. Datla, D. Doelling, V. Gärtner, T. Hewison, B. Iacovazzi, D. Kim, T. Kurino, J. Lafeuille, P. Minnis, D. Renaut, J. Schmetz, D. Tobin, L. Wang, F. Weng, X. Wu, F. Yu, P. Zhang, and T. Zhu, 2011: The Global Space-Based Inter-Calibration System. *Bull. Amer. Meteor. Soc.*, **92**, 467–475.

Goodman, S. J., J. Gurka, M. DeMaria, T. J. Schmit, A. Mostek, G. Jedlovec, C. Siewert, W. Feltz, J. Gerth, R. Brummer, S. Miller, B. Reed, and R. R. Reynolds, 2012: The GOES-R Proving Ground: Accelerating user readiness for the next-generation geostationary environmental satellite system. *Bull. Amer. Meteor. Soc.*, **93**, 1029–1040.

Gunshor, M. M., T. J. Schmit, W. P. Menzel, and D. C. Tobin, 2006: Intercalibration of the newest geostationary imagers via high spectral resolution AIRS data. Preprints, *14th Conf. on Satellite Meteorology and Oceanography*, Atlanta, USA, 6.13–6.13.

Heidinger, A., 2011: Algorithm theoretical basis document ABI cloud height. *NOAA NESDIS Center for Satellite Applications and Research*. [Available at http://www.goes-r.gov/resources/docs.html.]

Holmlund, K., 1998: The utilization of statistical properties of satellite-derived atmospheric motion vectors to derive quality indicators. *Wea. Forecasting*, **13**, 1093–1104.

Japan Meteorological Agency, 2013: *Outline of the operational numerical weather prediction at the Japan Meteorological Agency.* Appendix to WMO Technical Progress Report on the Global Data-processing and Forecasting System (GDPFS) and Numerical Weather Prediction (NWP) Research. Japan Meteorological Agency, Tokyo, Japan. [Available at http://www.jma.go.jp/jma/jma-eng/jma-center/nwp/outline2013-nwp/index.htm.]

JMA/MSC, 2006: *Summary of MSC system*. MSC technical note, Special Issue, 180 pp (in Japanese).

Johnson, R. X., and M. P. Weinreb, 1996: GOES-8 imager midnight effects and slope correction. Washwell, E. R. (ed.), *Proc. SPIE2812*, *GOES-8 and Beyond*, **2812**, 596–607.

Kawamoto, K., T. Nakajima, and T. Y. Nakajima, 2001: A global determination of cloud microphysics with AVHRR remote sensing. *J. Climate*, **14**, 2054–2068.

Kieffer, H. H., and T. C. Stone, 2005: The spectral irradiance of the moon. *Astron. J.*, **129**, 2887–2901.

Kishimoto, K., M. Sasaki, and M. Kunitsugu, 2013: *Cloud Grid Information Objective Dvorak Analysis (CLOUD) at the RSMC Tokyo - Typhoon Center*. Technical Review of RSMC Tokyo-Typhoon Center, **13**, 1–15.

Kobayashi, S., Y. Ota, Y. Harada, A. Ebita, M. Moriya, H. Onoda, K. Onogi, H. Kamahori, C. Kobayashi, H. Endo, K. Miyaoka, and K. Takahashi, 2015: The JRA-55 Reanalysis: General specifications and basic characteristics. *J. Meteor. Soc. Japan*, **93**, 5–48.

Kodaira, N., N. Murayama, H. Yamashita, and T. Kohno, 1978: On the Geostationary Meteorological Satellite, GMS (Himawari). *Tenki*, **25**, 245–268 (in Japanese).

Koenig, M., and E. de Coning, 2009: The MSG global instability indices product and its use as a nowcasting tool.

Wea. Forecasting, **24**, 272–285.

Kosaka, Y., A. Okuyama, H. Takenaka, and S. Fukuda, 2012: *Development and improvement of a vicarious calibration technique for the visible channel of geostationary meteorological satellites*. MSC technical note, **57**, 39–55 (in Japanese).

Lattanzio, A., J. Schulz, J. Matthews, A. Okuyama, B. Theodore, J. J. Bates, K. R. Knapp, Y. Kosaka, and L. Schüller, 2013: Land Surface Albedo from Geostationary Satelites: A multiagency collaboration within SCOPE-CM. *Bull. Amer. Meteor. Soc.*, **94**, 205–214.

Lee, Y., Z. Li, J. Li, and T. J. Schmit, 2014: Evaluation of the GOES-R ABI LAP retrieval algorithm using the GOES-13 sounder. *J. Atmos. Oceanic Technol.*, **31**, 3–19.

Majumdar, S. J., S. Aberson, C. Bishop, C. Cardinali, J. Caughey, A. Doerenbecher, P. Gauthier, R. Gelaro, T. Hamill, R. Langland, A. Lorenc, T. Nakazawa, F. Rabier, C. Reynolds, R. Saunders, Y. Song, Z. Toth, C. Velden, M. Weissmann, and C.-C. Wu, 2011: *Targeted observations for improving numerical weather prediction: An overview*. World Weather Research Programme / THORPEX Publication, **15**, 37 pp.

Maki, T., A. Ebita, T. Ishimizu, K. Nagata, M. Ikegami, and T. Sasaki, 2008: The daily 3D ozone produced by the chemical transport model for JRA-25. *Extended abstracts of the Third WCRP International Conference on Reanalysis*, Tokyo, Japan. [Available at http://wcrp.ipsl.jussieu.fr/Workshops/Reanalysis2008/abstract.html.]

Miyamura, K., 2007: *MTSAT-2 systems*. MSC technical note, **49**, 55–58 (in Japanese).

Menzel, W. P., W. L. Smith, and T. R. Stewart, 1983: Improved cloud motion wind vector and altitude assignment using VAS. *J. Climate Appl. Meteor.*, **22**, 377–384.

Meteo-France, 2012: *Algorithm theoretical basis document for "cloud products" (CMa-PGE01v3.2, CT-PGE02 v2.2 & CTTH-PGE03 v2.2)*. NWC SAF/MSG, 87 pp. [Available at http://www.nwcsaf.org/HD/MainNS.jsp.]

Mohr, T., 2014: Preparing the use of New generation geostationary meteorological satellites. *WMO Bull.*, **63**, 42–44.

Murata, H., M. Takahashi, and Y. Kosaka, 2015: *VIS and IR bands of Himawari-8/AHI compatible with those of MTSAT-2/Imager*. MSC technical note, **60**, 1–18.

Nakajima, T., and M. Tanaka, 1986: Matrix formulation for the transfer of solar radiation in a plane-parallel scattering atmosphere. *J. Quant. Spectrosc. Radiat. Transfer*, **35**, 13–21.

Nakajima, T., and M. Tanaka, 1988: Algorithms for radiative intensity calculations in moderately thick atmospheres using a truncation approximation. *J. Quant. Spectrosc. Radiat. Transfer*, **40**, 51–69.

Nakajima, T. Y., and T. Nakajima, 1995: Wide-area determination of cloud microphysical properties from NOAA AVHRR measurements for FIRE and ASTEX regions. *J. Atmos. Sci.*, **52**, 4043–4059.

Nakajima, T. Y., K. Suzuki, and G. L. Stephens, 2010a: Droplet growth in warm water clouds observed by the A-Train. Part I: Sensitivity analysis of the MODIS-derived cloud droplet sizes. *J. Atmos. Sci.*, **67**, 1884–1896.

Nakajima, T. Y., K. Suzuki, and G. L. Stephens, 2010b: Droplet growth in warm water clouds observed by the A-Train. Part II: A multisensor view. *J. Atmos. Sci.*, **67**, 1897–1907.

Nakazawa, T., K. Bessho, S. Hoshino, T. Komori, K. Yamashita, Y. Ohta, and K. Sato, 2010: THORPEX - Pacific Asian Regional Campaign (T-PARC). *Technical Review of RSMC Tokyo-Typhoon Center*, **12**, 1–4.

Ohshima, T., H. Uchida, T. Hamada, and S. Osano, 1991: A comparison of GMS cloud motion winds with ship-observed winds in typhoon vicinity. *Geophys. Mag.*, **44**, 27–36.

Okada, K., J. Heintzenberg, K. Kai, and Y. Qin, 2001: Shape of atmospheric mineral particles collected in three Chinese arid-regions. *J. Geophys. Res*. **28**, 3123–3126.

Okuyama, A., A. Andou, K. Date, K. Hosaka, N. Mori, H. Murata, T. Tabata, M. Takahashi, R. Yoshino, and K. Bessho, 2015: Preliminary validation of Himawari-8/AHI navigation and calibration. *Proc. SPIE 9607*, Earth Observing Systems XX, 96072E, doi:10.1117/12.2188978.

Olander, T. L., and C. S. Velden, 2007: The advanced Dvorak technique: Continued development of an objective scheme to estimate tropical cyclone intensity using geostationary infrared satellite imagery. *Wea. Forecasting*, **22**, 287–298.

Oyama, R., 2010: *Upgrade of atmospheric motion vector derivation algorithms at JMA/MSC*. MSC Technical Note, **50**, 1–32.

Pavolonis, M., and J. Sieglaff, 2012: GOES-R Advanced Baseline Imager (ABI) Algorithm Theoretical Basis Document For Volcanic Ash (Detection and Height). Version 3.0, *NOAA NESDIS Center for Satellite Applications and Research*. [Available at http://www.goes-r.gov/products/baseline-volcanic-ash.html.]

Prata, F., 2011: *Volcanic information derived from satellite data*. EUMETSAT volcanic ash and SO_2 pilot project report, EUMETSAT.

Remer, L. A., Y. J. Kaufman, D. Tanré, S. Mattoo, D. A. Chu, J. V. Martins, R.-R. Li, C. Ichoku, R. C. Levy, R. G. Kleidman, T. F. Eck, E. Vermote, and B. N. Holben, 2005: The MODIS aerosol algorithm, products, and validation. *J. Atmos. Sci.*, **62**, 947–973.

Saito, K., T. Fujita, Y. Yamada, J. Ishida, Y. Kumagai, K. Aranami, S. Ohmori, R. Nagasawa, S. Kumagai, C.

Muroi, T. Kato, H. Eito, and Y. Yamazaki, 2006: The operational JMA nonhydrostatic mesoscale model. *Mon. Wea. Rev.*, **134**, 1266–1298.

Schmetz, J., P. Pili, S. Tjemkes, D. Just, J. Kerkmann, S. Rota, and A. Ratier, 2002: An introduction to Meteosat Second Generation (MSG). *Bull. Amer. Meteor. Soc.*, **83**, 977–992.

Schmit, T. J., M. M. Gunshor, W. P. Menzel, J. J. Gurka, J. Li, and S. Bachmeier, 2005: Introducing the next-generation Advanced Baseline Imager on GOES-R. *Bull. Amer. Meteor. Soc.*, **86**, 1079–1096.

Schmit, T. J., J. Li, J. Li, W. F. Feltz, J. J. Gurka, M. D. Goldberg, and K. J. Schrab, 2008: The GOES-R Advanced Baseline Imager and the continuation of current sounder products. *J. Appl. Meteor. Climatol.*, **47**, 2696–2711.

Shimoji, K., 2014: Motion tracking and cloud height assignment methods for Himawari-8 AMV. *Proc. 12th Int. Winds Workshop*, University of Copenhagen, Danish Meteorological Institute, Copenhagen, Denmark, S2-07.

Stamnes, K., S. C. Tsay, W. Wiscombe, and K. Jayaweera, 1988: Numerically stable algorithm for discrete-ordinate-method radiative transfer in multiple scattering and emitting layered media. *Appl. Opt.*, **27**, 2502–2509.

Stohl, A., A. J. Prata, S. Eckhardt, L. Clarisse, A. Durant, S. Henne, N. I. Kristiansen, A. Minikin, U. Schumann, P. Seibert, K. Stebel, H. E. Thomas, T. Thorsteinsson, K. Tørseth, and B. Weinzierl, 2011: Determination of time- and height-resolved volcanic ash emissions and their use for quantitative ash dispersion modeling: The 2010 Eyjafjallajökull eruption. *Atmos. Chem. Phys.*, **11**, 4333–4351.

Sumida, Y., T. Imai, K. Mouri, and A. Sobajima, 2015: *Convective cloud information derivation algorithm theoretical basis document*. MSC technical note, submitted.

Szejwach, G., 1982: Determination of semi-transparent cirrus cloud temperature from infrared radiances: Application to METEOSAT. *J. Appl. Meteor.*, **21**, 384–393.

Tahara, Y., and K. Kato, 2009: *New spectral compensation method for intercalibration using high spectral resolution sounder*. MSC technical note, **52**, 1–37.

Takenaka, H., T. Y. Nakajima, A. Higurashi, A. Higuchi, T. Takamura, R. T. Pinker, and T. Nakajima, 2011: Estimation of solar radiation by neural network based on radiative transfer. *J. Geophys. Res.*, **116**, D08215, doi:10.1029/2009JD013337.

Tobin, D. C., H. E. Revercomb, C. C. Moeller, and T. S. Pagano, 2006: Use of Atmospheric Infrared Sounder high-spectral resolution spectra to assess the calibration of Moderate resolution Imaging Spectroradiometer on EOS Aqua. *J. Geophys. Res.*, **111**, D09S05, doi:10.1029/2005JD006 095.

Tsuchiyama, H., Y. Kurihara, and K. Masuda, 2013: Development of volcanic ash product for the next-generation Japanese Geostationary Meteorological Satellite Himawari-8. *Proc. 2013 EUMETSAT Meteorological Satellite Conference*, Vienna, Austria.

Uesawa, D., 2009: *Clear Sky Radiance (CSR) product from MTSAT-1R*. MSC technical note, **52**, 39–48.

Velden, C. S., T. L. Olander, and R. M. Zehr, 1998: Development of an objective scheme to estimate tropical cyclone intensity from digital geostationary satellite infrared imagery. *Wea. Forecasting*, **13**, 172–186.

Velden, C., B. Harper, F. Wells, J. L. Beven II, R. Zehr, T. Olander, M. Mayfield, C. C. Guard, M. Lander, R. Edson, L. Avila, A. Burton, M. Turk, A. Kikuchi, A. Christian, P. Caroff, and P. McCrone, 2006: The Dvorak tropical cyclone intensity estimation technique: A satellite-based method that has endured for over 30 years. *Bull. Amer. Meteor. Soc.*, **87**, 1195–1210.

Watts, P. D., R. Bennartz, and F. Fell, 2011: Retrieval of two-layer cloud properties from multispectral observations using optimal estimation. *J. Geophys. Res.*, **116**, D16203, doi:10.1029/2011JD015883.

Weinreb, M., and D. Han, 2003: Implementation of Midnight Blackbody Calibration Correction (MBCC). *NOAA NESDIS Office of Satellite Operations*. [Available at http://www.ospo.noaa.gov/Operations/GOES/calibration/mbcc_implemmentation.html.]

WMO, and EUMETSAT, 2007: Final report of RGB composite satellite imagery workshop. Boulder, United States. 14 pp.

Wu, T.-C., H. Liu, S. J. Majumdar, C. S. Velden, and J. L. Anderson, 2014: Influence of assimilating satellite-derived atmospheric motion vector observations on numerical analyses and forecasts of tropical cyclone track and intensity. *Mon. Wea. Rev.*, **142**, 49–71.

Xiong, X., W. L. Barnes, K. Chiang, H. Erives, N. Che, J. Sun, A. T. Isaacman, and V. V. Salomonson, 2004: Status of Aqua MODIS on-orbit calibration and characterization. *Proc. of SPIE*, **5570**, 317–327.

Yamashita, K., 2010: Observing system experiment of MTSAT-2 rapid scan atmospheric motion vector for T-PARC 2008 using the JMA operational NWP system. *Proc. 10th Int. Winds Workshop*, JMA, Tokyo, Japan, S6-06.

Yang, P., K. N. Liou, K. Wyser, and D. Mitchell, 2000: Parameterization of the scattering and absorption properties of individual ice crystals. *J. Geophys. Res.*, **105**, 4699–4718.